

FAST-PT II: an algorithm to calculate convolution integrals of general tensor quantities in cosmological perturbation theory

Xiao Fang, Jonathan A. Blazek, Joseph E. McEwen, and Christopher M. Hirata

Center for Cosmology and AstroParticle Physics, Department of Physics, The Ohio State University, 191 W Woodruff Ave, Columbus OH 43210, USA

E-mail: fang.307@osu.edu, blazek@berkeley.edu, mcewen.24@osu.edu, hirata.10@osu.edu

Abstract. Cosmological perturbation theory is a powerful tool to predict the statistics of large-scale structure in the weakly non-linear regime, but even at 1-loop order it results in computationally expensive mode-coupling integrals. Here we present a fast algorithm for computing 1-loop power spectra of quantities that depend on the observer's orientation, thereby generalizing the FAST-PT framework (McEwen *et al.*, 2016) that was originally developed for scalars such as the matter density. This algorithm works for an arbitrary input power spectrum and substantially reduces the time required for numerical evaluation. We apply the algorithm to four examples: intrinsic alignments of galaxies in the tidal torque model; the Ostriker-Vishniac effect; the secondary CMB polarization due to baryon flows; and the 1-loop matter power spectrum in redshift space. Code implementing this algorithm and these applications is publicly available at <https://github.com/JoeMcEwen/FAST-PT>.

Contents

1	Introduction	2
2	Method	3
2.1	Transformation To 1D Integrals	3
2.2	Algorithm	6
2.2.1	Implementation For $\mathcal{J}_{J_1 J_2 J_k}^{\alpha\beta}(k)$ Integral	6
2.2.2	Summary of the Algorithm	8
2.3	Removing Possible Divergences	9
2.3.1	Divergence From Kernel Expansions	9
2.3.2	Divergence From Periodic Power Spectrum and Choice of Bias Indices	9
3	Applications	10
3.1	Quadratic Intrinsic Alignments Model	11
3.1.1	Theory	11
3.1.2	Conversion to FAST-PT Format	12
3.2	Ostriker-Vishniac Effect	13
3.2.1	Theory	13
3.2.2	Conversion to FAST-PT Format	15
3.3	Kinetic polarization of the CMB	16
3.3.1	Theory	16
3.3.2	Conversion to FAST-PT Format	17
3.4	Redshift Space Distortions	17
3.4.1	Theory	17
3.4.2	Conversion to FAST-PT Format	20
4	Summary	22
A	Mathematical Identities	28
A.1	Spherical Harmonics and Legendre Polynomials	28
A.2	Wigner $3j$ and $6j$ Symbols	29
B	Derivations	30
B.1	Derivation of Eq. (2.3)	30
B.2	Derivation of Eq. (2.10) and (2.11)	31
C	Proof of Feasibility of Series Expansion	31

1 Introduction

Observational cosmology has entered a new era of precision measurement. Current and upcoming surveys [1–5] are enabling us to probe large-scale structure in more detail and over larger volumes, and hence to better constrain the underlying cosmological model. A parallel effort is underway to understand the astrophysical effects that are both signals and contaminants in these measurements. For example, weak gravitational lensing has become a powerful and direct probe of the dark matter distribution [6, 7], but it also suffers from systematic uncertainties, such as galaxy intrinsic alignments (IA), which must be mitigated in order to make use of high-precision measurements. Similarly, connecting observable tracers (*e.g.* in spectroscopic surveys) with the underlying dark matter requires a description of the bias relationship [8–12] and the effect of redshift-space distortions (RSDs) [13–15]. Developments in CMB measurements provide another illustration, as the range of observables has expanded from early initial detections of temperature anisotropies by COBE [16–24]. Current and future measurements [25–30] will be able to investigate more subtle effects, such as the kinetic Sunyaev-Zel’dovich (kSZ) [31, 32] and CMB spectral distortions [33, 34].

While modern cosmology has advanced significantly using our understanding from linear perturbation theory, nonlinear contributions become significant at late times and at smaller scales. In the quasi-linear regime, many relevant cosmological observables are usefully described using perturbation theory at higher order. Significant effort has been devoted to understanding structure formation via a range of perturbative techniques (*e.g.* [35–45]). In this work, we consider integrals in standard perturbation theory (SPT), although the methods and code we develop have a broader range of applications.

The next-to-leading-order (“1-loop”) corrections in these perturbative expansions are typically expressed as two-dimensional mode-coupling convolution integrals, which are generically time consuming to evaluate numerically. Recent algorithmic developments have dramatically sped up these computations for *scalar* quantities – those with no dependence on the direction of the observer, such as the matter density or real-space galaxy density. The new algorithms [46, 47] take advantage of the locality of evolution in perturbation theory, the scale invariance of cold dark matter (CDM) structure formation, and the Fast Fourier Transform (FFT); and work is underway to apply them to 2-loop power spectra as well [48]. In a previous paper, we introduced the FAST-PT implementation of these methods in Python [46].

However, there are many interesting 1-loop convolution integrals for *tensor* quantities – those with explicit dependence on the observer line of sight, such as those arising for redshift-space distortions. In this case, we need convolution integrals with “tensor” kernels:¹

$$I(k) = \int \frac{d^3\mathbf{q}_1}{(2\pi)^3} K(\hat{\mathbf{q}}_1 \cdot \hat{\mathbf{q}}_2, \hat{\mathbf{q}}_1 \cdot \hat{\mathbf{k}}, \hat{\mathbf{q}}_2 \cdot \hat{\mathbf{k}}, q_1, q_2) P(q_1) P(q_2) , \quad (1.1)$$

where $K(\hat{\mathbf{q}}_1 \cdot \hat{\mathbf{q}}_2, \hat{\mathbf{q}}_1 \cdot \hat{\mathbf{k}}, \hat{\mathbf{q}}_2 \cdot \hat{\mathbf{k}}, q_1, q_2)$ is a tensor mode-coupling kernel, $\mathbf{k} = \mathbf{q}_1 + \mathbf{q}_2$, $k = |\mathbf{k}|$, and $P(q)$ is the input signal – typically the linear matter power spectrum – logarithmically sampled in q . Due to the dependence on the direction of \mathbf{k} , the decomposition of these kernels is more complicated than in the scalar case. In this work, we generalize our FAST-PT algorithm

¹The kernel K can be expressed as a sum of polynomials in the relevant dot products. “Tensor” refers to the general transformation properties of the cosmological quantities being considered under a symmetry operation – in this case, rotations in $SO(3)$. For instance, the momentum density is a rank 1 tensor (a vector) while the IA field is a rank 2 tensor. The scalar case (rank 0) considered in [46] is thus a specific application of this more general framework.

to evaluate these tensor convolution integrals, achieving $\mathcal{O}(N \log N)$ performance as in the scalar case.

This paper is organized as follows: in §2 we provide the mathematical basis for our method (§2.1), introduce our algorithm (§2.2), and discuss divergences that may arise and how they are resolved (§2.3). In section §3 we apply our method to several examples: the quadratic intrinsic alignment model (§3.1); the Ostriker-Vishniac effect (§3.2); the kinetic polarization of CMB (§3.3); and the 1-loop redshift-space power spectrum (§3.4). Section §4 summarizes the results. An appendix contains derivations of the relevant mathematical identities. The Python code implementing this algorithm and the examples presented in this paper is publicly available at <https://github.com/JoemcEwen/FAST-PT>.

2 Method

In this section we extend the FAST-PT framework to include the computation of convolution integrals with tensor kernels in the form of Eq. (1.1)

Our approach is similar to the scalar version of FAST-PT. We first expand the kernel into several Legendre polynomial products – the explicit dependence on the direction $\hat{\mathbf{k}}$ requires an expansion in three angles rather than one (as shown in Eq. 2.1 and 2.2). Second, products of Legendre polynomials are written in spherical harmonics using the addition theorem, where the required combinations of spherical harmonics are constrained by Wigner $3j$ symbols and preserve angular momentum (as in Eq. 2.3). Third, in configuration space, the integral of each term in the expansion can be further transformed into a product of several one-dimensional integrals (as in Eq. 2.14 and 2.15), which can be quickly performed by assuming a (biased) log-periodic power spectrum and employing FFTs (as in Eq. 2.18 and 2.22).

We will first provide the theory in §2.1 and then briefly introduce our algorithm in §2.2. Finally, in §2.3 we will discuss physical divergence problems that can arise and the way to solve them through the choice of appropriate biasing of the log-periodic power spectrum.

2.1 Transformation To 1D Integrals

In general, the kernel function K can be decomposed as a summation of terms

$$K(\hat{\mathbf{q}}_1 \cdot \hat{\mathbf{q}}_2, \hat{\mathbf{q}}_1 \cdot \hat{\mathbf{k}}, \hat{\mathbf{q}}_2 \cdot \hat{\mathbf{k}}, q_1, q_2) = \sum_{\ell_1, \ell_2, \ell, \alpha, \beta} A_{\ell_1 \ell_2 \ell}^{\alpha \beta} \mathcal{P}_\ell(\hat{\mathbf{q}}_1 \cdot \hat{\mathbf{q}}_2) \mathcal{P}_{\ell_1}(\hat{\mathbf{k}} \cdot \hat{\mathbf{q}}_2) \mathcal{P}_{\ell_2}(\hat{\mathbf{k}} \cdot \hat{\mathbf{q}}_1) q_1^\alpha q_2^\beta, \quad (2.1)$$

where \mathcal{P}_ℓ are the Legendre polynomials, and the $A_{\ell_1 \ell_2 \ell}^{\alpha \beta}$ coefficients specify the components of a particular kernel. For general angular dependences the sum may require an infinite number of terms. However the kernels that appear in CDM perturbation theory and galaxy biasing theory are composed of a finite number of terms in a polynomial expansion. This decomposition leads us to consider integrals of the form

$$f(k) = \int \frac{d^3 \mathbf{q}_1}{(2\pi)^3} \mathcal{P}_\ell(\hat{\mathbf{q}}_1 \cdot \hat{\mathbf{q}}_2) \mathcal{P}_{\ell_1}(\hat{\mathbf{k}} \cdot \hat{\mathbf{q}}_2) \mathcal{P}_{\ell_2}(\hat{\mathbf{k}} \cdot \hat{\mathbf{q}}_1) q_1^\alpha q_2^\beta P(q_1) P(q_2). \quad (2.2)$$

The product of Legendre polynomials can be decomposed into spherical harmonics by the addition theorem. Using the result presented in Appendix B.1, we can write the product of three Legendre polynomials in terms of spherical harmonics and Wigner $3j$ symbols:

$$\begin{aligned} & \mathcal{P}_\ell(\hat{\mathbf{q}}_1 \cdot \hat{\mathbf{q}}_2) \mathcal{P}_{\ell_2}(\hat{\mathbf{q}}_1 \cdot \hat{\mathbf{k}}) \mathcal{P}_{\ell_1}(\hat{\mathbf{q}}_2 \cdot \hat{\mathbf{k}}) \\ &= \sum_{J_1, J_2, J_k} C_{\ell_1 \ell_2 \ell}^{J_1 J_2 J_k} \sum_{M_1, M_2, M_k} Y_{J_1 M_1}(\hat{\mathbf{q}}_1) Y_{J_2 M_2}(\hat{\mathbf{q}}_2) Y_{J_k M_k}(\hat{\mathbf{k}}) \begin{pmatrix} J_1 & J_2 & J_k \\ M_1 & M_2 & M_k \end{pmatrix}, \quad (2.3) \end{aligned}$$

with coefficients given by

$$C_{\ell_1 \ell_2 \ell}^{J_1 J_2 J_k} = (4\pi)^{3/2} (-1)^{\ell_1 + \ell_2 + \ell} \times \sqrt{(2J_1 + 1)(2J_2 + 1)(2J_k + 1)} \begin{pmatrix} J_1 & \ell_2 & \ell \\ 0 & 0 & 0 \end{pmatrix} \begin{pmatrix} \ell_1 & J_2 & \ell \\ 0 & 0 & 0 \end{pmatrix} \begin{pmatrix} \ell_1 & \ell_2 & J_k \\ 0 & 0 & 0 \end{pmatrix} \left\{ \begin{matrix} J_1 & J_2 & J_k \\ \ell_1 & \ell_2 & \ell \end{matrix} \right\}, \quad (2.4)$$

where we have used the $3j$ and $6j$ symbols, denoted by $\begin{pmatrix} \cdot & \cdot & \cdot \\ \cdot & \cdot & \cdot \end{pmatrix}$ and $\left\{ \begin{matrix} \cdot & \cdot & \cdot \\ \cdot & \cdot & \cdot \end{matrix} \right\}$, respectively. The integers M_1, M_2, M_k satisfy the selection rule $M_1 + M_2 + M_k = 0$. The coefficients $C_{\ell_1 \ell_2 \ell}^{J_1 J_2 J_k}$ map the product of spherical harmonics in Eq. (2.3), written in terms of the J_1, J_2, J_k basis, to the original ℓ_1, ℓ_2, ℓ basis of Legendre polynomials. Upon replacing the product of Legendre polynomials in Eq. (2.2) with Eq. (2.3) (omitting the coefficients $C_{\ell_1 \ell_2 \ell}^{J_1 J_2 J_k}$), we arrive at an integral over the product of three spherical harmonics, which we will denote as $I_{J_1 J_2 J_k}^{\alpha\beta}(\mathbf{k})$. For each combination of J_1, J_2, J_k , we have

$$I_{J_1 J_2 J_k}^{\alpha\beta}(\mathbf{k}) = \sum_{M_1 M_2 M_k} \int \frac{d^3 \mathbf{q}_1}{(2\pi)^3} P(q_1) P(q_2) Y_{J_1 M_1}(\hat{\mathbf{q}}_1) Y_{J_2 M_2}(\hat{\mathbf{q}}_2) Y_{J_k M_k}(\hat{\mathbf{k}}) q_1^\alpha q_2^\beta \begin{pmatrix} J_1 & J_2 & J_k \\ M_1 & M_2 & M_k \end{pmatrix} \equiv \sum_{M_k} Y_{J_k M_k}(\hat{\mathbf{k}}) T_{J_1 J_2 J_k M_k}^{\alpha\beta}(\mathbf{k}), \quad (2.5)$$

where we have defined

$$T_{J_1 J_2 J_k M_k}^{\alpha\beta}(\mathbf{k}) \equiv \sum_{M_1 M_2} \begin{pmatrix} J_1 & J_2 & J_k \\ M_1 & M_2 & M_k \end{pmatrix} H_{J_1 M_1 J_2 M_2}^{\alpha\beta}(\mathbf{k}) \quad \text{and} \quad (2.6)$$

$$H_{J_1 M_1 J_2 M_2}^{\alpha\beta}(\mathbf{k}) \equiv \int \frac{d^3 \mathbf{q}_1}{(2\pi)^3} P(q_1) P(q_2) Y_{J_1 M_1}(\hat{\mathbf{q}}_1) Y_{J_2 M_2}(\hat{\mathbf{q}}_2) q_1^\alpha q_2^\beta. \quad (2.7)$$

We can separate $H_{J_1 M_1 J_2 M_2}^{\alpha\beta}(\mathbf{k})$ into a product of two integrals, respectively over \mathbf{q}_1 and \mathbf{q}_2 , by Fourier transforming to configuration space

$$H_{J_1 M_1 J_2 M_2}^{\alpha\beta}(\mathbf{r}) = \int \frac{d^3 \mathbf{q}_1}{(2\pi)^3} \frac{d^3 \mathbf{q}_2}{(2\pi)^3} e^{i(\mathbf{q}_1 + \mathbf{q}_2) \cdot \mathbf{r}} q_1^\alpha q_2^\beta P(q_1) P(q_2) Y_{J_1 M_1}(\hat{\mathbf{q}}_1) Y_{J_2 M_2}(\hat{\mathbf{q}}_2) = \bar{H}_{J_1 J_2}^{\alpha\beta}(\mathbf{r}) Y_{J_1 M_1}(\hat{\mathbf{r}}) Y_{J_2 M_2}(\hat{\mathbf{r}}), \quad (2.8)$$

where we have used the plane wave expansion (Eq. A.5) together with orthogonality relations (Eq. A.3) to arrive at the equality. We have also defined

$$\bar{H}_{J_1 J_2}^{\alpha\beta}(\mathbf{r}) \equiv \frac{(4\pi)^{2i^{J_1+J_2}}}{(2\pi)^6} \int_0^\infty dq_1 q_1^{2+\alpha} P(q_1) j_{J_1}(q_1 r) \int_0^\infty dq_2 q_2^{2+\beta} P(q_2) j_{J_2}(q_2 r), \quad (2.9)$$

where $j_J(qr)$ are the spherical Bessel functions. Substituting Eq. (2.8) into the definition of $T_{J_1 J_2 J_k M_k}^{\alpha\beta}$ we obtain

$$\begin{aligned} T_{J_1 J_2 J_k M_k}^{\alpha\beta}(\mathbf{r}) &= \sum_{M_1 M_2} \begin{pmatrix} J_1 & J_2 & J_k \\ M_1 & M_2 & M_k \end{pmatrix} H_{J_1 M_1 J_2 M_2}^{\alpha\beta}(\mathbf{r}) \\ &= \bar{H}_{J_1 J_2}^{\alpha\beta}(\mathbf{r}) \sum_{M_1 M_2} \begin{pmatrix} J_1 & J_2 & J_k \\ M_1 & M_2 & M_k \end{pmatrix} Y_{J_1 M_1}(\hat{\mathbf{r}}) Y_{J_2 M_2}(\hat{\mathbf{r}}) \\ &= \bar{H}_{J_1 J_2}^{\alpha\beta}(\mathbf{r}) a_{J_1 J_2 J_k} Y_{J_k M_k}^*(\hat{\mathbf{r}}), \end{aligned} \quad (2.10)$$

where

$$a_{J_1 J_2 J_k} \equiv \sqrt{\frac{(2J_1 + 1)(2J_2 + 1)}{4\pi(2J_k + 1)}} \begin{pmatrix} J_1 & J_2 & J_k \\ 0 & 0 & 0 \end{pmatrix}. \quad (2.11)$$

The derivation of Eqs. (2.10) and (2.11) is provided in Appendix (B.2). Fourier transforming back to k -space, we obtain

$$\begin{aligned} T_{J_1 J_2 J_k M_k}^{\alpha\beta}(\mathbf{k}) &= \int d^3r T_{J_1 J_2 J_k M_k}^{\alpha\beta}(\mathbf{r}) e^{-i\mathbf{k}\cdot\mathbf{r}} \\ &= a_{J_1 J_2 J_k} \int r^2 dr \bar{H}_{J_1 J_2}^{\alpha\beta}(r) \int d^2\hat{\mathbf{r}} Y_{J_k M_k}^*(\hat{\mathbf{r}}) e^{-i\mathbf{k}\cdot\mathbf{r}} \\ &= a_{J_1 J_2 J_k} \int r^2 dr \bar{H}_{J_1 J_2}^{\alpha\beta}(r) \int d^2\hat{\mathbf{r}} Y_{J_k M_k}^*(\hat{\mathbf{r}}) 4\pi \sum_{\ell' m'} (-i)^{\ell'} j_{\ell'}(kr) Y_{\ell' m'}^*(\hat{\mathbf{k}}) Y_{\ell' m'}(\hat{\mathbf{r}}) \\ &= a_{J_1 J_2 J_k} \int r^2 dr \bar{H}_{J_1 J_2}^{\alpha\beta}(r) 4\pi \sum_{\ell' m'} (-i)^{\ell'} j_{\ell'}(kr) Y_{\ell' m'}^*(\hat{\mathbf{k}}) \delta_{\ell' J_k} \delta_{m' M_k} \\ &= 4\pi (-i)^{J_k} a_{J_1 J_2 J_k} \int r^2 dr \bar{H}_{J_1 J_2}^{\alpha\beta}(r) j_{J_k}(kr) Y_{J_k M_k}^*(\hat{\mathbf{k}}), \end{aligned} \quad (2.12)$$

where in the third equality we have used the plane wave expansion (Eq. A.5), and in the fourth equality used the orthogonality relation between spherical harmonics (Eq. A.3). Combining the results from Eq. (2.9), (2.12), (2.11), we arrive at

$$\begin{aligned} I_{J_1 J_2 J_k}^{\alpha\beta}(k) &= 4\pi (-i)^{J_k} a_{J_1 J_2 J_k} \int r^2 dr \bar{H}_{J_1 J_2}^{\alpha\beta}(r) j_{J_k}(kr) \sum_{M_k} Y_{J_k M_k}(\hat{\mathbf{k}}) Y_{J_k M_k}^*(\hat{\mathbf{k}}) \\ &= (-i)^{J_k} (2J_k + 1) a_{J_1 J_2 J_k} \int r^2 dr \bar{H}_{J_1 J_2}^{\alpha\beta}(r) j_{J_k}(kr) \\ &= (-1)^{J_k + (J_1 + J_2 + J_k)/2} \sqrt{\frac{(2J_1 + 1)(2J_2 + 1)(2J_k + 1)}{64\pi^9}} \begin{pmatrix} J_1 & J_2 & J_k \\ 0 & 0 & 0 \end{pmatrix} \\ &\quad \times \int r^2 dr J_{J_1 J_2}^{\alpha\beta}(r) j_{J_k}(kr), \end{aligned} \quad (2.13)$$

where $J_1 + J_2 + J_k$ must be even for the $3j$ symbol to be non-zero, and $J_{J_1 J_2}^{\alpha\beta}(r)$ is defined by

$$J_{J_1 J_2}^{\alpha\beta}(r) \equiv \left[\int_0^\infty dq_1 q_1^{2+\alpha} P(q_1) j_{J_1}(q_1 r) \right] \left[\int_0^\infty dq_2 q_2^{2+\beta} P(q_2) j_{J_2}(q_2 r) \right]. \quad (2.14)$$

Combining Eq. (2.13) and (2.3) we can rewrite the integral (2.2) as

$$\begin{aligned} &\int \frac{d^3\mathbf{q}_1}{(2\pi)^3} \mathcal{P}_\ell(\hat{\mathbf{q}}_1 \cdot \hat{\mathbf{q}}_2) \mathcal{P}_{\ell_1}(\hat{\mathbf{k}} \cdot \hat{\mathbf{q}}_2) \mathcal{P}_{\ell_2}(\hat{\mathbf{k}} \cdot \hat{\mathbf{q}}_1) q_1^\alpha q_2^\beta P(q_1) P(q_2) \\ &= \sum_{J_1, J_2, J_k} C_{\ell_1 \ell_2 \ell}^{J_1 J_2 J_k} I_{J_1 J_2 J_k}^{\alpha\beta}(k) = \sum_{J_1, J_2, J_k} B_{\ell_1 \ell_2 \ell}^{J_1 J_2 J_k} \int r^2 dr J_{J_1 J_2}^{\alpha\beta}(r) j_{J_k}(kr), \end{aligned} \quad (2.15)$$

where the coefficients $B_{\ell_1 \ell_2 \ell}^{J_1 J_2 J_k}$ are given by

$$\begin{aligned}
B_{\ell_1 \ell_2 \ell}^{J_1 J_2 J_k} &\equiv C_{\ell_1 \ell_2 \ell}^{J_1 J_2 J_k} (-1)^{J_k + (J_1 + J_2 + J_k)/2} \sqrt{\frac{(2J_1 + 1)(2J_2 + 1)(2J_k + 1)}{64\pi^9}} \begin{pmatrix} J_1 & J_2 & J_k \\ 0 & 0 & 0 \end{pmatrix} \\
&= (-1)^{\ell + \frac{J_1 + J_2 + J_k}{2}} \times \frac{(2J_1 + 1)(2J_2 + 1)(2J_k + 1)}{\pi^3} \\
&\quad \times \begin{pmatrix} J_1 & \ell_2 & \ell \\ 0 & 0 & 0 \end{pmatrix} \begin{pmatrix} \ell_1 & J_2 & \ell \\ 0 & 0 & 0 \end{pmatrix} \begin{pmatrix} \ell_1 & \ell_2 & J_k \\ 0 & 0 & 0 \end{pmatrix} \begin{pmatrix} J_1 & J_2 & J_k \\ 0 & 0 & 0 \end{pmatrix} \left\{ \begin{matrix} J_1 & J_2 & J_k \\ \ell_1 & \ell_2 & \ell \end{matrix} \right\}. \quad (2.16)
\end{aligned}$$

The evaluation of $J_{J_1 J_2}^{\alpha\beta}(r)$ is similar to the analogous quantity in scalar FAST-PT. For notational simplicity, we define the last integral in Eq. (2.15) as

$$\mathcal{J}_{J_1 J_2 J_k}^{\alpha\beta}(k) = \int r^2 dr J_{J_1 J_2}^{\alpha\beta}(r) j_{J_k}(kr). \quad (2.17)$$

Eq. (2.17) is similar in structure to Eq. (2.19) of [46]. As such, we can easily generalize the FAST-PT framework to evaluate integrals in the form of Eq. (2.17).

Note that some (scalar) 2-loop integrals have similar structure to the tensor 1-loop integrals considered here. In recent work, Ref. [48] employed similar techniques involving Wigner $6j$ symbols to deal with these 2-loop integrals, although the implementations are somewhat different.

2.2 Algorithm

2.2.1 Implementation For $\mathcal{J}_{J_1 J_2 J_k}^{\alpha\beta}(k)$ Integral

We adopt the discrete Fourier transformation of the power spectrum as discussed in the first FAST-PT paper [46],

$$c_m = W_m \sum_{q=0}^{N-1} \frac{P(k_q)}{k_q^{\nu_1}} e^{-2\pi i m q/N} \quad \rightarrow \quad P_{\text{filtered}}(k_q) = \sum_{m=-N/2}^{N/2} c_m k_q^{\nu_1 + i\eta_m}, \quad (2.18)$$

where N is the size of the input power spectrum, $\eta_m = m \times 2\pi/(N\Delta)$, $m = -N/2, -N/2 + 1, \dots, N/2 - 1, N/2$, ν_1 is the bias index, and Δ is the linear spacing, *i.e.* $k_q = k_0 \exp(q\Delta)$ with k_0 being the smallest value in the k array. Similarly, c'_n are the Fourier coefficients of the power spectrum with bias index ν_2 . The physics of the bias has been discussed in [46]² and the choice of its value will be discussed in §2.3.2. For a real power spectrum the Fourier coefficients obey $c_m^* = c_{-m}$, $c'_n{}^* = c'_{-n}$. W_m is a window function³ used to smooth the edges of the Fourier coefficient array of the biased power spectrum (*e.g.* from the cutoffs in k), hence smoothing over the noise and sharp features in the power spectrum, as well as prevent them from propagating non-locally in the “filtered” power spectrum. The “filtered” power spectrum is then treated as the input power spectrum and its c_m ’s are used for calculations afterwards.

²The bias is introduced to solve the numerical divergences arising from the Fourier transform. By performing the Fourier transform, we assume the input power spectrum to be periodic, so that there are infinite “satellite” power spectra on both low and high k sides. To avoid infinite contribution from the satellites, appropriate bias values are required.

³The window function we use is a smoothing function described in Appendix C of [46].

Following Eq. (2.17) in [46], we can write Eq. (2.14) as⁴

$$J_{J_1 J_2}^{\alpha\beta}(r) = \frac{\pi}{2} \sum_{m=-N/2}^{N/2} \sum_{n=-N/2}^{N/2} c_m c'_n g_{\alpha m} g_{\beta n} 2^{Q_{\alpha m} + Q_{\beta n}} r^{-6 - \nu_1 - \nu_2 - \alpha - \beta - i\eta_m - i\eta_n}, \quad (2.19)$$

where $g_{\alpha m} \equiv g(J_1 + \frac{1}{2}, Q_{\alpha m})$, $g_{\beta n} \equiv g(J_2 + \frac{1}{2}, Q_{\beta n})$, $Q_{\alpha m} \equiv \frac{3}{2} + \nu_1 + \alpha + i\eta_m$, $Q_{\beta n} \equiv \frac{3}{2} + \nu_2 + \beta + i\eta_n$, and

$$g(\mu, \kappa) \equiv \frac{\Gamma[(\mu + \kappa + 1)/2]}{\Gamma[(\mu - \kappa + 1)/2]}. \quad (2.20)$$

The integral then becomes

$$\begin{aligned} \mathcal{J}_{J_1 J_2 J_k}^{\alpha\beta}(k_q) &\equiv \int_0^\infty dr r^2 J_{J_1 J_2}^{\alpha\beta}(r) j_{J_k}(k_q r) \\ &= \frac{\pi}{2} \sum_{m=-N/2}^{N/2} \sum_{n=-N/2}^{N/2} c_m g_{\alpha m} c'_n g_{\beta n} 2^{Q_{\alpha m} + Q_{\beta n}} \int_0^\infty dr j_{J_k}(k_q r) r^{-4 - \nu_1 - \nu_2 - \alpha - \beta - i\eta_m - i\eta_n} \\ &= \frac{\pi}{2} \sum_{m=-N/2}^{N/2} \sum_{n=-N/2}^{N/2} c_m g_{\alpha m} c'_n g_{\beta n} 2^{Q_{\alpha m} + Q_{\beta n}} k_q^{Q_{\alpha m} + Q_{\beta n}} \int_0^\infty dr j_{J_k}(r) r^{-4 - \nu_1 - \nu_2 - \alpha - \beta - i\eta_m - i\eta_n} \\ &= \left(\frac{\pi}{2}\right)^{\frac{3}{2}} \sum_{m=-N/2}^{N/2} \sum_{n=-N/2}^{N/2} c_m g_{\alpha m} c'_n g_{\beta n} 2^{Q_{\alpha m} + Q_{\beta n}} k_q^{Q_{\alpha m} + Q_{\beta n}} \\ &\quad \times \int_0^\infty dr J_{J_k + \frac{1}{2}}(r) r^{-\frac{9}{2} - \nu_1 - \nu_2 - \alpha - \beta - i\eta_m - i\eta_n} \\ &= \left(\frac{\pi}{2}\right)^{\frac{3}{2}} \sum_{m=-N/2}^{N/2} \sum_{n=-N/2}^{N/2} c_m g_{\alpha m} c'_n g_{\beta n} 2^{Q_{\alpha m} + Q_{\beta n}} k_q^{Q_{\alpha m} + Q_{\beta n}} \\ &\quad \times 2^{-\frac{9}{2} - \nu_1 - \nu_2 - \alpha - \beta - i\eta_m - i\eta_n} g\left(J_k + \frac{1}{2}, -\frac{9}{2} - \nu_1 - \nu_2 - \alpha - \beta - i\eta_m - i\eta_n\right) \\ &= \frac{\pi^{3/2}}{8} \sum_{m=-N/2}^{N/2} \sum_{n=-N/2}^{N/2} c_m g_{\alpha m} c'_n g_{\beta n} k_q^{Q_{\alpha m} + Q_{\beta n}} g\left(J_k + \frac{1}{2}, -\frac{9}{2} - \nu_1 - \nu_2 - \alpha - \beta - i\eta_m - i\eta_n\right). \end{aligned} \quad (2.21)$$

We define $\tau_h \equiv \eta_m + \eta_n$ and $Q_h \equiv Q_{\alpha m} + Q_{\beta n}$, which only depends on the sum $m + n$. We write the double summation over m and n as a discrete convolution, indexed by h , such that

⁴The major step is substituting the expansions of the power spectra into Eq. (2.14), and utilizing the formula: $\int_0^\infty dt t^\kappa J_\mu(t) = 2^\kappa g(\mu, \kappa)$ for $\Re \kappa < 1/2$, $\Re(\kappa + \mu) > -1$, where the Bessel function of the first kind J_μ is related to the spherical Bessel function by $J_\mu(t) = \sqrt{2t/\pi} j_{\mu-1/2}(t)$, and $g(\mu, \kappa)$ is defined in Eq. (2.20).

$h = m + n = \{-N, -N + 1, \dots, N - 1, N\}$. This leads to

$$\begin{aligned}
\mathcal{J}_{J_1 J_2 J_k}^{\alpha\beta}(k_q) &= \frac{\pi^{3/2}}{8} \sum_{m=-N/2}^{N/2} \sum_{n=-N/2}^{N/2} c_m g_{\alpha m} c'_n g_{\beta n} k_q^{Q_h} g\left(J_k + \frac{1}{2}, -Q_h - \frac{3}{2}\right) \\
&= \frac{\pi^{3/2}}{8} \sum_h [c_m g_{\alpha m} \otimes c'_n g_{\beta n}]_h k_q^{Q_h} g\left(J_k + \frac{1}{2}, -Q_h - \frac{3}{2}\right) \\
&= \frac{\pi^{3/2}}{8} k_q^{3+\nu_1+\nu_2+\alpha+\beta} \sum_h C_h \exp(i\tau_h \ln k_0) \exp(i\tau_h q \Delta) g\left(J_k + \frac{1}{2}, -Q_h - \frac{3}{2}\right) \\
&= \frac{\pi^{3/2}}{8} k_q^{3+\nu_1+\nu_2+\alpha+\beta} \text{IFFT} \left[C_h g\left(J_k + \frac{1}{2}, -Q_h - \frac{3}{2}\right) \right], \tag{2.22}
\end{aligned}$$

where C_h is defined as the convolution in the second equality, and IFFT is the discrete inverse Fast Fourier Transform. This derivation is similar to Eq. (2.21) in [46].

In the algorithm, for each set of (J_1, J_2, J_k) there are 3 FFT operations and 1 convolution. In our public code, we use the `scipy.signal.fftconvolve` routine [49] to perform the convolution, which uses the convolution theorem, resulting in 3 additional FFT operations. Thus, for each set of (J_1, J_2, J_k) there are 6 FFT operations executed in total.

2.2.2 Summary of the Algorithm

From Eq (2.15), the tensor convolution integral (1.1) can be decomposed as

$$I(k) = \sum_{\ell_1, \ell_2, \ell, \alpha, \beta} A_{\ell_1 \ell_2 \ell}^{\alpha\beta} \sum_{J_1, J_2, J_k} B_{\ell_1 \ell_2 \ell}^{J_1 J_2 J_k} \int r^2 dr J_{J_1 J_2}^{\alpha\beta}(r) j_{J_k}(kr). \tag{2.23}$$

Our algorithm is thus as follows:

1. Given an integral in the form of Eq. (1.1), expand it in terms of Eq. (2.2) to obtain all the non-zero coefficients $A_{\ell_1 \ell_2 \ell}^{\alpha\beta}$;
2. For each combination of ℓ_1, ℓ_2, ℓ , use Eq. (2.16) to calculate all the possible combinations of J_1, J_2, J_k and their corresponding (non-zero) coefficients $B_{\ell_1 \ell_2 \ell}^{J_1 J_2 J_k}$;
3. For all the possible combinations of J_1, J_2, J_k , calculate $J_{J_1 J_2}^{\alpha\beta}(r)$ and perform the Hankel transform integration (see §2.2.1 for the detailed implementation);
4. Sum up all the terms to obtain the result.

The criteria for non-zero $B_{\ell_1 \ell_2 \ell}^{J_1 J_2 J_k}$ can be obtained from the properties of the Wigner 3j symbols. From Eq. (2.16) we have

$$|\ell_1 - \ell_2| \leq J_k \leq \ell_1 + \ell_2, \quad |\ell - \ell_2| \leq J_1 \leq \ell + \ell_2, \quad |\ell - \ell_1| \leq J_2 \leq \ell + \ell_1, \tag{2.24}$$

$$|J_1 - J_2| \leq J_k \leq J_1 + J_2, \tag{2.25}$$

and

$$J_1 + \ell_2 + \ell = \text{even}, \quad \ell_1 + J_2 + \ell = \text{even}, \quad \ell_1 + \ell_2 + J_k = \text{even}. \tag{2.26}$$

The condition that “ $J_1 + J_2 + J_k = \text{even}$ ” is redundant since it can be inferred from the conditions (Eq. 2.26).⁵

⁵Summing up the three equations in Eq. (2.26) we have $J_1 + J_2 + J_k + 2(\ell_1 + \ell_2 + \ell) = \text{even}$, which leads to $J_1 + J_2 + J_k = \text{even}$.

2.3 Removing Possible Divergences

Note that the algorithm we have presented in this section is only for the “ $P_{22}(k)$ ”-type integrals, *i.e.* containing two power spectra $P(q_1)P(q_2)$ in the integrand as in Eq. (1.1). In §3.4.2 we will encounter integrals containing $P(q_1)P(k)$ or $P(q_2)P(k)$, which can be reduced to one-dimensional integrals, analogous to $P_{13}(k)$ in 1-loop SPT (for details on our algorithm of P_{22} and P_{13} , see [46]). We first focus on the $P_{22}(k)$ -type integrals, where two potential types of divergence may emerge in this algorithm.

2.3.1 Divergence From Kernel Expansions

When we expand the kernel into the Legendre polynomial form, the integral (2.2) can be divergent for some combinations of $\ell, \ell_1, \ell_2, \alpha, \beta$, even though the sum of all terms will be convergent for physical observables. If the input power spectrum is the linear matter power spectrum $P_{\text{lin}}(k)$, for $q_1 \gg k$, $\mathbf{q}_2 \approx -\mathbf{q}_1$, and the power spectra, $P_{\text{lin}}(q_1)$ and $P_{\text{lin}}(q_2)$, both scale as q_1^{-3} . Thus the integral (2.2) is proportional to $\int dq_1 q_1^{\alpha+\beta-4}$ for $\ell_1 = \ell_2$. Convergence requires that $\alpha + \beta < 3$. For $\ell_1 \neq \ell_2$, this constraint is relaxed due to suppression from the angular integral.

For $q_1 \ll k$, $\mathbf{q}_2 \approx \mathbf{k}$, so that $P_{\text{lin}}(q_1) \propto q_1^{n_s}$ and $P_{\text{lin}}(q_2) \propto k^{n_{\text{eff}}(k)}$, where $n_s \sim 1$ is the primordial spectral index of the matter power spectrum, and $n_{\text{eff}}(k)$ is the effective spectral index at k . The integral is then proportional to $\int dq_1 q_1^{\alpha+n_s+2}$, leading to the requirement: $\alpha > -3 - n_s$ for $\ell = \ell_2$. Similarly, for q_2 small, we get $\beta > -3 - n_s$ for $\ell = \ell_1$. As before, these constraints are relaxed if $\ell \neq \ell_2$ or $\ell \neq \ell_1$.

Violations of these criteria have to be removed by regularization, specifically canceling the divergent parts. None of the examples in the next section have such a divergence (although see §3.4.2 for a discussion of a separate numerical divergence which is treated analytically).

2.3.2 Divergence From Periodic Power Spectrum and Choice of Bias Indices

As discussed in [46], the use of FFTs enforces a periodic power spectrum which can lead to unphysical divergences for certain choices of the power-law bias. This generalized implementation of FAST-PT has more freedom in the choice of bias indices ν_1, ν_2 , compared with the original “scalar” version. First, it allows the use of two different bias indices ν_1, ν_2 for the two input power spectra, instead of one fixed ν . Second, it allows the bias indices to change for different Legendre integrals (2.2). We now discuss our choice of ν_1, ν_2 .

In FAST-PT, we expand the input power spectra $P_{\text{lin}}(q_1), P_{\text{lin}}(q_2)$ into sums over power-law spectra $q_1^{\nu_1+i\eta m}$ and $q_2^{\nu_2+i\eta n}$. The real parts of the exponents, *i.e.* the bias indices ν_1, ν_2 , will affect the convergence of the integrals.

Using a similar argument as in the previous subsection, for large q_1 , we will have $P_{\text{lin}}(q_1) \propto q_1^{\nu_1}, P_{\text{lin}}(q_2) \propto q_1^{\nu_2}$. Working out the integral, we end up with the criterion: $\nu_1 + \alpha + \nu_2 + \beta < -3$ for $\ell_1 = \ell_2$. For small q_1 , we get $\alpha + \nu_1 > -3$ for $\ell = \ell_2$; similarly for small q_2 , we get $\beta + \nu_2 > -3$ for $\ell = \ell_1$. These constraints are relaxed if $\ell \neq \ell_2$ or $\ell \neq \ell_1$. We plot the convergence region in Figure 1.

In our code, we take $\nu_1 = -2 - \alpha$ and $\nu_2 = -2 - \beta$ for all cases to satisfy the above conditions. Note that the choice of different bias values for different components of a given observable is technically non-physical since the choice of bias specifies the properties of the “universe in which the calculation is done. However, if the input k -range (or zero-padding) is

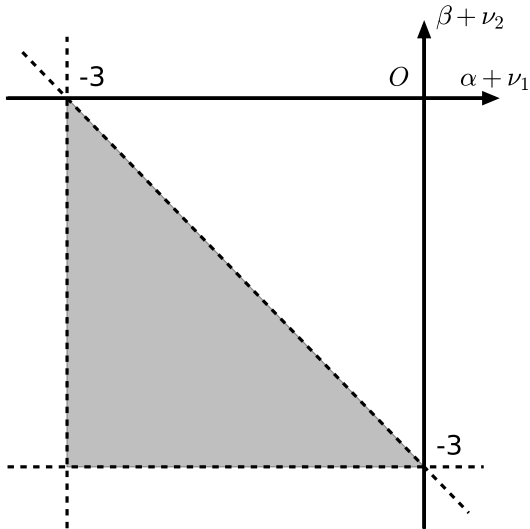


Figure 1. The convergence region of the bias indices ν_1, ν_2 is indicated by the shaded region.

sufficient, this effect is negligible on scales of interest⁶. The fixed biasing scheme ($\nu = -2$) employed for scalar quantities in [46] avoids this issue. However, because one component of P_{22} violates $\alpha + \nu > -3$ (for $\ell = 0$) under this fixed biasing, we required analytic regularization to enforce Galilean invariance and remove the formally infinite contribution to displacements from $k \rightarrow 0$ modes. Those integrals can be performed using the new scheme without the analytic regularization, although in this case a larger input range in k (or additional zero-padding) is required for numerical convergence.

3 Applications

In this section we apply the FAST-PT tensor algorithm to several cosmological applications: the quadratic intrinsic alignment model (§3.1); the Ostriker-Vishniac effect (§3.2); the kinetic polarization of CMB (§3.3); and the 1-loop redshift-space distortion power spectrum (§3.4). In each subsection we first briefly review the theory behind the application before expanding the relevant integral(s) into the form of Eq. (2.2) and comparing the output for each case with the results from conventional (and significantly slower) two-dimensional cubature integration. To

⁶In principle, different bias indices could lead to slightly different integral results due to contributions from the periodic “satellite” power spectra. However, when the input k -range or zero-padding is sufficient, these artificial contributions become negligible. When the bias indices are chosen inside the convergence region in Fig. 1, we can always find a sufficient k -range, while outside the region, there may be no sufficient range. To test the stability of the results, we compared the OV power spectrum (Eq. 3.9) obtained using the bias indices $\nu_1 = -2 - \alpha, \nu_2 = -2 - \beta$ to the result obtained with the indices $\nu_1 = -2.5 - \alpha, \nu_2 = -2.5 - \beta$, and found that the maximum fractional difference over the range 0.003-10 h/Mpc is less than 3×10^{-7} .

demonstrate the performance of the code, we provide this comparison out to high wavenumbers ($k = 10 h/\text{Mpc}$). We caution that the underlying perturbative models are not applicable to the real Universe beyond the mildly nonlinear regime ($k \sim \text{few} \times 10^{-1} h/\text{Mpc}$), even though FAST-PT can still accurately compute the perturbation theory integrals. We envision these examples both as results in and of themselves, and, more importantly, as reference material for other cosmologists who may want to compute 1-loop power spectra with their own kernels and convert them to FAST-PT format.

Our input linear power spectrum was generated by CAMB [50], assuming a flat Λ CDM cosmology corresponding to the Planck 2015 results [51]. We used Python version 3.5.1, NUMPY 1.10.4, and SCIPY 0.17.0. The public code is also compatible with Python 2.

3.1 Quadratic Intrinsic Alignments Model

3.1.1 Theory

Weak gravitational lensing has become one of the most promising probes of the dark matter distribution [5, 52]. The observed shapes of galaxies are weakly distorted (“sheared”) by the gravitational potential of the large-scale structure along the line of sight. Correlations in observed shapes tell us about the projected matter distribution. However, weak lensing suffers from several systematic effects, one of which is intrinsic correlations between galaxy ellipticities, known as “intrinsic alignments” (IA) [53, 54]. In the weak lensing regime, the intrinsic shapes of galaxies dominate the observed shapes (*i.e.* are much larger than the lensing shear contribution). While the dominant uncorrelated component of intrinsic ellipticities does not affect the correlation of shapes beyond adding noise, the component correlating the ellipticity with the underlying tidal field can bias cosmological inference from weak lensing measurements [55]. On the other hand, IA can also serve as a probe of the cosmological density field as well as the astrophysics of galaxies and halos [56].

On large scales, there are two types of physically-motivated intrinsic galaxy alignment models, the tidal (linear) and quadratic alignment models [57, 58]. The tidal alignment model is based on the assumption that large-scale correlations in the intrinsic ellipticity field of triaxial elliptical galaxies are linearly related to fluctuations in the primordial gravitational tidal field in which the galaxy formed.⁷ In quadratic models (often referred to as “tidal torquing”), the observed ellipticity of spiral galaxies comes from the inclination of the disk with respect to the line of sight, and hence from the direction of its angular momentum. In this scenario, the tidal field from the large-scale structure will both “spin-up” the galaxy as well as provide a torque, contributing to the mean intrinsic ellipticity at second order. In general, once nonlinear effects are included, both tidal alignment and tidal torquing models have contributions from mode coupling integrals of the form of Eq. 1.1 [59]. More generally, these models can be viewed as components in an “effective expansion” of IA [60], analogous to treatments of galaxy biasing [61].

In the quadratic alignment model [57], the intrinsic alignment E/B -mode power spectrum $P_{\tilde{\gamma}_I}^{(EE, BB)}(k)$ contains a convolution integral in the form of

$$P_{\text{IA,quad}}^{(EE, BB)}(k) = 2 \int \frac{d^3 \mathbf{q}_1}{(2\pi)^3} h_{(E, B)}^2(\hat{\mathbf{q}}_1, \hat{\mathbf{q}}_2) P_{\text{lin}}(q_1) P_{\text{lin}}(q_2), \quad (3.1)$$

⁷Similar results are obtained from assuming that intrinsic shapes are “instantaneously” set by the tidal field at the time of observation (see [59] for further discussion).

where $\mathbf{k} = \mathbf{q}_1 + \mathbf{q}_2$ and h_E and h_B are tensor kernels. If we choose the coordinate system such that $\hat{\mathbf{k}} = \hat{\mathbf{z}}$ and $\hat{\mathbf{x}}$ points to the observer, $h_{(E,B)}$ can be expressed as

$$\begin{aligned} h_E(\hat{\mathbf{q}}_1, \hat{\mathbf{q}}_2) &= h_{zz}(\hat{\mathbf{q}}_1, \hat{\mathbf{q}}_2) - h_{yy}(\hat{\mathbf{q}}_1, \hat{\mathbf{q}}_2) \\ &= (\hat{\mathbf{q}}_1 \cdot \hat{\mathbf{q}}_2)(\hat{\mathbf{q}}_1 \cdot \hat{\mathbf{k}})(\hat{\mathbf{q}}_2 \cdot \hat{\mathbf{k}}) - \frac{1}{3}(\hat{\mathbf{q}}_1 \cdot \hat{\mathbf{k}})^2 - \frac{1}{3}(\hat{\mathbf{q}}_2 \cdot \hat{\mathbf{k}})^2 \\ &\quad - (\hat{\mathbf{q}}_1 \cdot \hat{\mathbf{q}}_2)(\hat{\mathbf{q}}_1 \cdot \hat{\mathbf{y}})(\hat{\mathbf{q}}_2 \cdot \hat{\mathbf{y}}) + \frac{1}{3}(\hat{\mathbf{q}}_1 \cdot \hat{\mathbf{y}})^2 + \frac{1}{3}(\hat{\mathbf{q}}_2 \cdot \hat{\mathbf{y}})^2, \end{aligned} \quad (3.2)$$

$$\begin{aligned} h_B(\hat{\mathbf{q}}_1, \hat{\mathbf{q}}_2) &= 2h_{zy}(\hat{\mathbf{q}}_1, \hat{\mathbf{q}}_2) \\ &= \left[(\hat{\mathbf{q}}_1 \cdot \hat{\mathbf{q}}_2)(\hat{\mathbf{q}}_2 \cdot \hat{\mathbf{k}}) - \frac{2}{3}(\hat{\mathbf{q}}_1 \cdot \hat{\mathbf{k}}) \right] (\hat{\mathbf{q}}_1 \cdot \hat{\mathbf{y}}) \\ &\quad + \left[(\hat{\mathbf{q}}_1 \cdot \hat{\mathbf{q}}_2)(\hat{\mathbf{q}}_1 \cdot \hat{\mathbf{k}}) - \frac{2}{3}(\hat{\mathbf{q}}_2 \cdot \hat{\mathbf{k}}) \right] (\hat{\mathbf{q}}_2 \cdot \hat{\mathbf{y}}) \end{aligned} \quad (3.3)$$

where we can see that $h_{(E,B)}$ have $\hat{\mathbf{k}}$ dependence. We have made the Limber approximation in assuming that only modes transverse to the line of sight will contribute to observed correlations, hence $\hat{\mathbf{n}} = \hat{\mathbf{x}}$. Note that our choice of the coordinate system is different from the conventions in some previous work where $\hat{\mathbf{z}}$ is chosen to be along the line of sight. Because the integrand has an azimuthal symmetry around \mathbf{k} , independent of the line-of-sight direction, it is more convenient to work in our coordinate system, although the final results do not depend on this choice.

3.1.2 Conversion to FAST-PT Format

In spherical coordinates, we have $\hat{\mathbf{q}}_i = (\sin \theta_i \cos \phi_i, \sin \theta_i \sin \phi_i, \cos \theta_i)$ for $i = 1, 2$. Note that $\phi_1 = \phi_2 - \pi \equiv \phi$ because \mathbf{q}_1 and \mathbf{q}_2 add up to \mathbf{k} which is on the z -axis. We obtain

$$\begin{aligned} \hat{\mathbf{q}}_1 \cdot \hat{\mathbf{y}} &= \sin \theta_1 \sin \phi, & \hat{\mathbf{q}}_2 \cdot \hat{\mathbf{y}} &= -\sin \theta_2 \sin \phi, \\ \hat{\mathbf{q}}_1 \cdot \hat{\mathbf{q}}_2 &= \cos \theta_1 \cos \theta_2 - \sin \theta_1 \sin \theta_2, \\ (\hat{\mathbf{q}}_1 \cdot \hat{\mathbf{y}})(\hat{\mathbf{q}}_2 \cdot \hat{\mathbf{y}}) &= \left(\hat{\mathbf{q}}_1 \cdot \hat{\mathbf{q}}_2 - (\hat{\mathbf{q}}_1 \cdot \hat{\mathbf{k}})(\hat{\mathbf{q}}_2 \cdot \hat{\mathbf{k}}) \right) \sin^2 \phi, \\ (\hat{\mathbf{q}}_1 \cdot \hat{\mathbf{y}})^2 + (\hat{\mathbf{q}}_2 \cdot \hat{\mathbf{y}})^2 &= \left(2 - (\hat{\mathbf{q}}_1 \cdot \hat{\mathbf{k}})^2 - (\hat{\mathbf{q}}_2 \cdot \hat{\mathbf{k}})^2 \right) \sin^2 \phi. \end{aligned} \quad (3.4)$$

Now we can rewrite h_E as

$$\begin{aligned} h_E(\hat{\mathbf{q}}_1, \hat{\mathbf{q}}_2) &= (\hat{\mathbf{q}}_1 \cdot \hat{\mathbf{q}}_2)(\hat{\mathbf{q}}_1 \cdot \hat{\mathbf{k}})(\hat{\mathbf{q}}_2 \cdot \hat{\mathbf{k}})(1 + \sin^2 \phi) - (\hat{\mathbf{q}}_1 \cdot \hat{\mathbf{q}}_2)^2 \sin^2 \phi \\ &\quad - \frac{1}{3}(1 + \sin^2 \phi) \left[(\hat{\mathbf{q}}_1 \cdot \hat{\mathbf{k}})^2 + (\hat{\mathbf{q}}_2 \cdot \hat{\mathbf{k}})^2 \right] + \frac{2}{3} \sin^2 \phi \\ &= \mu \mu_1 \mu_2 (1 + \sin^2 \phi) - \mu^2 \sin^2 \phi - \frac{1}{3}(1 + \sin^2 \phi)(\mu_1^2 + \mu_2^2) + \frac{2}{3} \sin^2 \phi, \end{aligned} \quad (3.5)$$

where we define $\mu \equiv \hat{\mathbf{q}}_1 \cdot \hat{\mathbf{q}}_2$, $\mu_1 \equiv \hat{\mathbf{q}}_2 \cdot \hat{\mathbf{k}}$, $\mu_2 \equiv \hat{\mathbf{q}}_1 \cdot \hat{\mathbf{k}}$ (following the convention where each angle is labeled by the subscript for the opposite side in the triangle).

ℓ	ℓ_1	ℓ_2	$A_{\ell_1 \ell_2 \ell}^{00(E)}$	$A_{\ell_1 \ell_2 \ell}^{00(B)}$
0	0	0	16/81	-41/405
	2	0	713/1134	-298/567
	2	2	95/162	-40/81
	4	0	38/315	-32/315
1	1	1	-107/60	59/45
	3	1	-19/15	16/15
2	0	0	239/756	-2/9
	2	0	11/9	-20/27
	2	2	19/27	-16/27
3	1	1	-7/10	2/5
4	0	0	3/35	—

Table 1. The coefficient of each term in the Legendre polynomial expansion of h_E^2 and h_B^2 kernels (without the factor of 2 in front of the integral Eq. 3.1). Due to symmetry, we need only keep terms with $\ell_1 \geq \ell_2$ (multiplying the value by two where relevant).

Taking square of h_E and then averaging over ϕ , we obtain⁸

$$\begin{aligned}
h_E^2 &= \frac{1}{6} - \frac{1}{2}\mu^2 + \frac{3}{8}\mu^4 - \frac{7}{18}(\mu_1^2 + \mu_2^2) + \frac{7}{12}\mu^2(\mu_1^2 + \mu_2^2) + \frac{19}{72}(\mu_1^4 + \mu_2^4) \\
&\quad + \frac{7}{6}\mu\mu_1\mu_2 - \frac{7}{4}\mu^3\mu_1\mu_2 - \frac{19}{12}\mu(\mu_1^3\mu_2 + \mu_1\mu_2^3) + \frac{19}{36}\mu_1^2\mu_2^2 + \frac{19}{8}\mu^2\mu_1^2\mu_2^2 \\
&= \sum_{\substack{\ell_1, \ell_2, \ell \\ \ell_1 \geq \ell_2}} A_{\ell_1 \ell_2 \ell}^{00(E)} \mathcal{P}_\ell(\mu) \mathcal{P}_{\ell_1}(\mu_1) \mathcal{P}_{\ell_2}(\mu_2), \tag{3.6}
\end{aligned}$$

where we apply the symmetry between \mathbf{q}_1 and \mathbf{q}_2 and only keep terms with $\ell_1 \geq \ell_2$. Similarly, we can write h_B^2 kernel in the same form with coefficients $A_{\ell_1 \ell_2 \ell}^{00(B)}$. The coefficient of each term is listed in Table 1. Now each term has been expressed in the required form of $q_1^\alpha q_2^\beta \mathcal{P}_\ell(\mu) \mathcal{P}_{\ell_1}(\mu_1) \mathcal{P}_{\ell_2}(\mu_2)$, with $\alpha = \beta = 0$.

In Figure 2, we show the FAST-PT result of $P_{\text{IA,quad}}^{(EE, BB)}(k)$ (Eq. 3.1) and the fractional difference comparing to the results from conventional methods. The plot shows excellent agreement between two methods, with fractional accuracy better than 3×10^{-5} up to $k = 10 \text{ h/Mpc}$.

3.2 Ostriker-Vishniac Effect

3.2.1 Theory

After CMB photons leave the surface of last scattering, they can experience further interactions, leading to secondary anisotropies. One of the most important is re-scattering off of free electrons after reionization in which photons can be shifted to higher or lower frequencies due to motions of the electrons. The thermal Sunyaev-Zel'dovich effect (tSZ) results from thermal motion of the electrons, usually in galaxy clusters as these are the hottest regions. Bulk hydrodynamic motions produce the kinetic Sunyaev-Zel'dovich (kSZ) effect (in clusters)

⁸Averaging over the azimuthal angle, we have $\langle \cos^2 \phi \rangle = \frac{1}{2\pi} \int_0^{2\pi} d\phi \cos^2 \phi = 1/2$, $\langle \cos^4 \phi \rangle = \frac{1}{2\pi} \int_0^{2\pi} d\phi \cos^4 \phi = 3/8$. More generally, $\langle \cos^{2n} \phi \rangle = \pi^{-\frac{1}{2}} \Gamma(n + \frac{1}{2}) / \Gamma(n + 1)$ for any non-negative integer n , known as the Wallis formula.

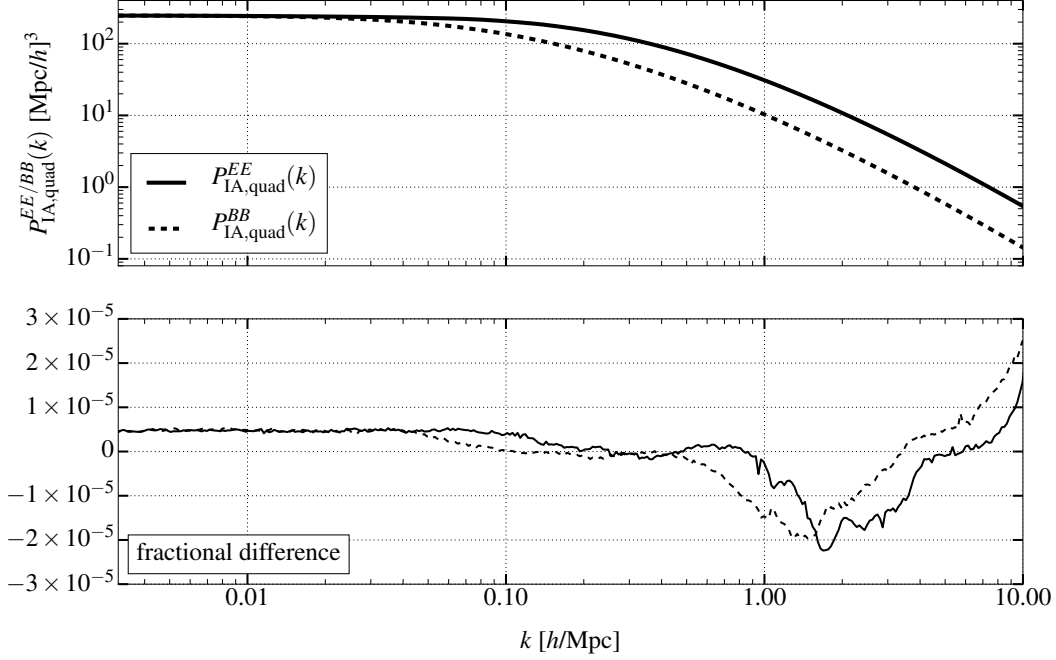


Figure 2. The FAST-PT result for the intrinsic alignment integrals $P_{\text{IA,quad}}^{(EE, BB)}(k)$ in Eq. (3.1) (upper panel) and the fractional difference compared to the conventional method (lower panel).

or the Ostriker-Vishniac (OV) effect (in large-scale structure). In this section, we consider the second-order perturbation theory analysis of the Ostriker-Vishniac effect.

The fractional temperature perturbation in the direction $\hat{\mathbf{n}}$ on the sky is given by [62–64]

$$\Theta(\hat{\mathbf{n}}) = - \int_0^{\eta_0} dw g(w) \hat{\mathbf{n}} \cdot \mathbf{q}(\mathbf{w}) , \quad (3.7)$$

where $\mathbf{q}(\mathbf{w}) \equiv [1 + \delta(\mathbf{w})]\mathbf{v}(\mathbf{w})$, $\mathbf{v}(\mathbf{w})$ is the bulk velocity at position $\mathbf{w} \equiv w\hat{\mathbf{n}}$ at a comoving distance w (or a conformal time $\eta_0 - w$), $g(w)$ is the visibility function specifying the probability distribution for scattering from reionized electrons, given by $g(w) = (d\tau/dw)e^{-\tau}$, and τ is the optical depth.

At 1-loop, the angular power spectrum of Θ produced by the OV effect, $C_\ell^{\Theta\Theta}$ (equivalent to $P_p(\kappa)$ in [64]), requires the calculation of the Vishniac power spectrum, which is a tensor convolution integral. In a flat Universe,

$$C_\ell^{\Theta\Theta} = \frac{1}{16\pi^2} \int_0^{\eta_0} \frac{(a(w)g(w))^2}{w^2} \left(\frac{\dot{D}D}{D_0} \right)^2 S(\ell/w) dw , \quad (3.8)$$

where D and D_0 are the growth factors at w and at present, respectively. Choosing the same coordinate system as in the IA calculation above, *i.e.* $\hat{\mathbf{z}} = \hat{\mathbf{k}}$ and $\hat{\mathbf{x}}$ pointing to the observer, the integral is given by

$$S(k) = 4\pi^2 \int \frac{d^3\mathbf{q}_1}{(2\pi)^3} \left(\frac{q_{1x}}{q_1^2} + \frac{q_{2x}}{q_2^2} \right)^2 P_{\text{lin}}(q_1) P_{\text{lin}}(q_2) , \quad (3.9)$$

which is consistent with Eq. (21) in [64]. Our interest here is in fast computation of $S(k)$.

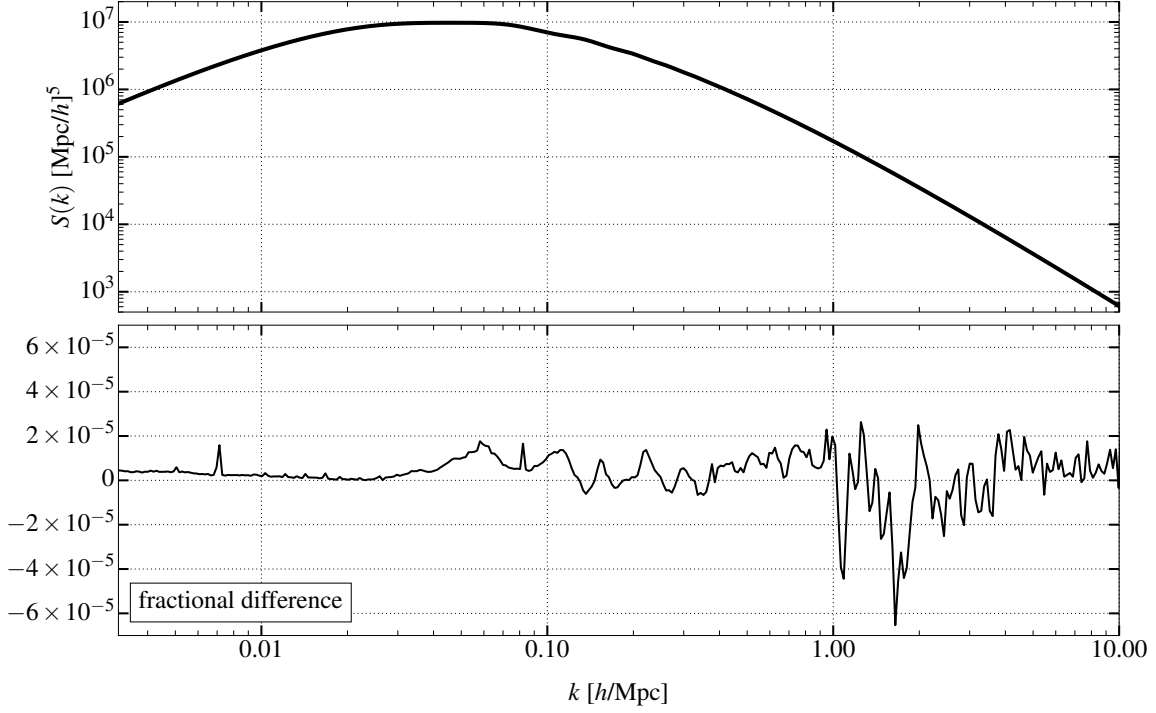


Figure 3. The FAST-PT result for the Ostriker-Vishniac effect integral $S(k)$ in Eq. (3.9) (upper panel) and the fractional difference compared to the conventional method (lower panel).

3.2.2 Conversion to FAST-PT Format

First noting that the integral $S(k)$ is symmetric under the exchange $\mathbf{q}_1 \leftrightarrow \mathbf{q}_2$ and that $q_{2x} = -q_{1x}$, we can expand Eq. (3.9) as

$$S(k) = 4\pi^2 \int \frac{d^3 \mathbf{q}_1}{(2\pi)^3} \left(\frac{2q_{1x}^2}{q_1^4} - \frac{2q_{1x}^2}{q_1^2 q_2^2} \right) P_{\text{lin}}(q_1) P_{\text{lin}}(q_2). \quad (3.10)$$

In the spherical coordinate system, $q_{1x}^2 = q_1^2 \sin^2 \theta \cos^2 \phi$, which becomes $\frac{1}{2} q_1^2 \sin^2 \theta$ after averaging over ϕ . The kernel is thus

$$\left(1 - (\hat{\mathbf{k}} \cdot \hat{\mathbf{q}}_1)^2\right) \left(\frac{1}{q_1^2} - \frac{1}{q_2^2}\right) = \frac{2}{3} [\mathcal{P}_0(\mu_2) - \mathcal{P}_2(\mu_2)] \left(\frac{1}{q_1^2} - \frac{1}{q_2^2}\right), \quad (3.11)$$

where $\mu_2 \equiv \hat{\mathbf{k}} \cdot \hat{\mathbf{q}}_1$. There are 4 terms in this case: $A_{000}^{-2,0} = 2/3$, $A_{020}^{-2,0} = -2/3$, $A_{000}^{0,-2} = -2/3$, $A_{020}^{0,-2} = 2/3$.⁹

In Figure 3, we show the FAST-PT result of $S(k)$ integral (Eq. 3.9) and the fractional difference from a conventional method. The plot shows excellent agreement between two methods with accuracy better than 6×10^{-5} up to $k = 10 h/\text{Mpc}$.

⁹It is possible to write the integral $S(k)$ in other forms without breaking the $\mathbf{q}_1 \leftrightarrow \mathbf{q}_2$ symmetry, *e.g.* to write the kernel as $(1 - \mu_2^2) \left(\frac{1}{2q_1^2} - \frac{1}{q_2^2} + \frac{q_1^2}{2q_2^4}\right)$. However, the q_2^{-4} terms suffer from divergence at small q_2 (see §2.3). The divergence is artificial because $1 - \mu_2^2 \rightarrow 0$ when $q_2 \rightarrow 0$, which makes physical sense, but it can cause instability in the FAST-PT code.

3.3 Kinetic polarization of the CMB

3.3.1 Theory

The kSZ effect can induce a secondary linear polarization in the CMB via the quadratic Doppler effect and Thomson scattering [65, 66]. Due to the motion of baryons, an isotropic CMB appears to have a quadrupole anisotropy component in the rest frame of the scattering baryons, as seen from the expansion

$$\Theta = \frac{\sqrt{1 - v_b^2}}{1 - \hat{\mathbf{n}} \cdot \mathbf{v}_b} - 1 \simeq \hat{\mathbf{n}} \cdot \mathbf{v}_b + (\hat{\mathbf{n}} \cdot \mathbf{v}_b)^2 - \frac{1}{2}v_b^2, \quad (3.12)$$

where Θ is the fractional temperature fluctuation of CMB in the direction of $\hat{\mathbf{n}}$ as seen by the scattering electron. The relation between the quadrupole anisotropy at position \mathbf{x} and the CMB temperature angular distribution seen by the scatter is given by

$$Q^{(m)}(\mathbf{x}) = - \int d\Omega \frac{Y_{2m}^*(\hat{\mathbf{n}})}{\sqrt{4\pi}} \Theta(\mathbf{x}, \hat{\mathbf{n}}), \quad (3.13)$$

where $m = 0, \pm 1, \pm 2$. In the Rayleigh-Jeans limit,¹⁰ the observed power spectra of E - and B -mode polarizations are related to the power spectra of $Q^{(0,\pm 2)}$ and $Q^{(\pm 1)}$, respectively, by

$$\begin{aligned} C_\ell^{EE} &= \frac{3\pi^2}{10\ell^3} \int dw g^2 D_A \left(\frac{3}{4} \Delta_Q^{2(0)}(k) + \frac{1}{8} \sum_{m=\pm 2} \Delta_Q^{2(m)}(k) \right) \quad \text{and} \\ C_\ell^{BB} &= \frac{3\pi^2}{10\ell^3} \int dw g^2 D_A \left(\frac{1}{2} \sum_{m=\pm 1} \Delta_Q^{2(m)}(k) \right), \end{aligned} \quad (3.14)$$

where $\Delta_Q^{2(m)}(k) = k^3 P^{(m)}(k)/(2\pi^2)$ is the variance of $Q^{(m)}$ per unit range in $\ln k$, the spherical harmonics in Eq. (3.13) are evaluated with \mathbf{k} on the z -axis, g is the visibility function, and the comoving angular distance $D_A = w$ (the comoving distance) in a flat Universe. Since the quadrupole anisotropy arises from the quadratic Doppler effect, in Fourier space with $\hat{\mathbf{k}} = \hat{\mathbf{z}}$, we have

$$Q^{(m)}(\mathbf{k}) = - \int d\Omega \frac{Y_{2m}^*(\hat{\mathbf{n}})}{\sqrt{4\pi}} \int \frac{d^3 \mathbf{q}_1}{(2\pi)^3} \hat{\mathbf{n}} \cdot \mathbf{v}_b(\mathbf{q}_1) \hat{\mathbf{n}} \cdot \mathbf{v}_b(\mathbf{q}_2), \quad (3.15)$$

where \mathbf{v}_b is the baryon bulk velocity. In linear theory

$$\dot{\delta} = - \frac{\nabla \cdot \mathbf{v}_b}{a} = fH\delta, \quad (3.16)$$

where $f \equiv d \ln G / d \ln a$ for growth factor G and scale factor a . Taking the Fourier transform and assuming no vorticity, we obtain

$$\mathbf{v}_b(\mathbf{k}) = ia f H \frac{\delta(\mathbf{k})}{k} \hat{\mathbf{k}} \equiv iT \frac{\delta(\mathbf{k})}{k} \hat{\mathbf{k}}. \quad (3.17)$$

¹⁰This limit is necessary to justify saying that *temperature* is scattered – really it is the intensity, but at low frequencies the two are proportional. As noted in Ref. [65], the kinetic polarization has a specific non-blackbody spectral shape, which can be used to scale from the Rayleigh-Jeans limit to any frequency of interest.

Substituting Eq. (3.17) into Eq. (3.15) and applying identities (A.1, A.11), we have

$$\begin{aligned}
Q^{(m)}(\mathbf{k}) &= \frac{T^2}{\sqrt{4\pi}} \int \frac{d^3\mathbf{q}_1}{(2\pi)^3} \frac{\delta(\mathbf{q}_1)\delta(\mathbf{q}_2)}{q_1q_2} \int d\Omega Y_{2m}^*(\hat{\mathbf{n}}) (\hat{\mathbf{n}} \cdot \hat{\mathbf{q}}_1) (\hat{\mathbf{n}} \cdot \hat{\mathbf{q}}_2) \\
&= \frac{T^2}{\sqrt{4\pi}} \int \frac{d^3\mathbf{q}_1}{(2\pi)^3} \frac{\delta(\mathbf{q}_1)\delta(\mathbf{q}_2)}{q_1q_2} \int d\Omega Y_{2m}^*(\hat{\mathbf{n}}) \left(\frac{4\pi}{3}\right)^2 \sum_{m_1m_2} Y_{1m_1}(\hat{\mathbf{q}}_1) Y_{1m_1}^*(\hat{\mathbf{n}}) Y_{1m_2}(\hat{\mathbf{q}}_2) Y_{1m_2}^*(\hat{\mathbf{n}}) \\
&= \frac{T^2}{\sqrt{4\pi}} \int \frac{d^3\mathbf{q}_1}{(2\pi)^3} \frac{\delta(\mathbf{q}_1)\delta(\mathbf{q}_2)}{q_1q_2} \left(\frac{4\pi}{3}\right)^2 \sum_{m_1m_2} Y_{1m_1}(\hat{\mathbf{q}}_1) Y_{1m_2}(\hat{\mathbf{q}}_2) \sqrt{\frac{45}{4\pi}} \begin{pmatrix} 2 & 1 & 1 \\ 0 & 0 & 0 \end{pmatrix} \begin{pmatrix} 2 & 1 & 1 \\ m & m_1 & m_2 \end{pmatrix} \\
&= \frac{T^2}{\sqrt{4\pi}} \left(\frac{4\pi}{3}\right)^2 \sqrt{\frac{3}{2\pi}} \int \frac{d^3\mathbf{q}_1}{(2\pi)^3} \frac{\delta(\mathbf{q}_1)\delta(\mathbf{q}_2)}{q_1q_2} \sum_{m_1m_2} Y_{1m_1}(\hat{\mathbf{q}}_1) Y_{1m_2}(\hat{\mathbf{q}}_2) \begin{pmatrix} 2 & 1 & 1 \\ m & m_1 & m_2 \end{pmatrix}.
\end{aligned} \tag{3.18}$$

Following the definition that $\langle Q^{(m)}(\mathbf{k})Q^{(m)}(\mathbf{k}') \rangle = (2\pi)^3 P_{Q^{(m)}}(k) \delta_D^3(\mathbf{k} + \mathbf{k}')$, we have

$$P^{(m)}(k) \equiv \frac{27P_{Q^{(m)}}(k)}{4(4\pi)^2T^4} = \int \frac{d^3\mathbf{q}_1}{(2\pi)^3} \frac{P_{\text{lin}}(q_1)P_{\text{lin}}(q_2)}{q_1^2q_2^2} \left| \sum_{m_1m_2} Y_{1m_1}(\hat{\mathbf{q}}_1) Y_{1m_2}(\hat{\mathbf{q}}_2) \begin{pmatrix} 2 & 1 & 1 \\ m & m_1 & m_2 \end{pmatrix} \right|^2, \tag{3.19}$$

which is a tensor convolution integral in the form of Eq. (2.2).

3.3.2 Conversion to FAST-PT Format

Since $\mathbf{k} \parallel \hat{\mathbf{z}}$, the kernels for each m can be written in terms of μ, μ_1, μ_2 . Note that m_1, m_2 can only be 0 or ± 1 , so we can explicitly write down all the spherical harmonics and Wigner $3j$ symbols in the summation and transform to Legendre polynomial products as before:

$$\begin{aligned}
m = 0 : & \quad \frac{q_1^{-2}q_2^{-2}}{80\pi^2} [2 + 6\mathcal{P}_2(\mu_1) + \mathcal{P}_2(\mu) + 6\mathcal{P}_2(\mu_1)\mathcal{P}_2(\mu_2) - 9\mathcal{P}_1(\mu_1)\mathcal{P}_1(\mu_2)\mathcal{P}_1(\mu)], \\
m = \pm 1 : & \quad \frac{q_1^{-2}q_2^{-2}}{160\pi^2} [1 - 2\mathcal{P}_2(\mu_1) + 9\mathcal{P}_1(\mu_1)\mathcal{P}_1(\mu_2)\mathcal{P}_1(\mu) - 8\mathcal{P}_2(\mu_1)\mathcal{P}_2(\mu_2)], \\
m = \pm 2 : & \quad \frac{q_1^{-2}q_2^{-2}}{80\pi^2} [1 - 2\mathcal{P}_2(\mu_1) + \mathcal{P}_2(\mu_1)\mathcal{P}_2(\mu_2)].
\end{aligned} \tag{3.20}$$

Note that the symmetry between μ_1 and μ_2 has been used to simplify the kernels. The coefficients $A_{\ell_1\ell_2\ell}^{\alpha\beta}$ are now trivially seen.

In Figure 4, we show the FAST-PT result of $P^{(m)}(k)$ integrals (Eq. 3.19) for $m = 0, \pm 1, \pm 2$, respectively, and the fractional difference from a conventional method. The plots show excellent agreement between two methods with accuracy better than 6×10^{-5} in the k range from 0.01 to 10 h/Mpc .

3.4 Redshift Space Distortions

3.4.1 Theory

Cosmological surveys map large-scale structure in three dimensions, using galaxies or other luminous tracers of the total matter distribution (e.g. [1–5]). To determine distance along the line-of-sight, surveys typically use redshift information and are thus actually making a map in “redshift space.” In order to compare theory to galaxy redshift survey data, models must be translated into redshift space.

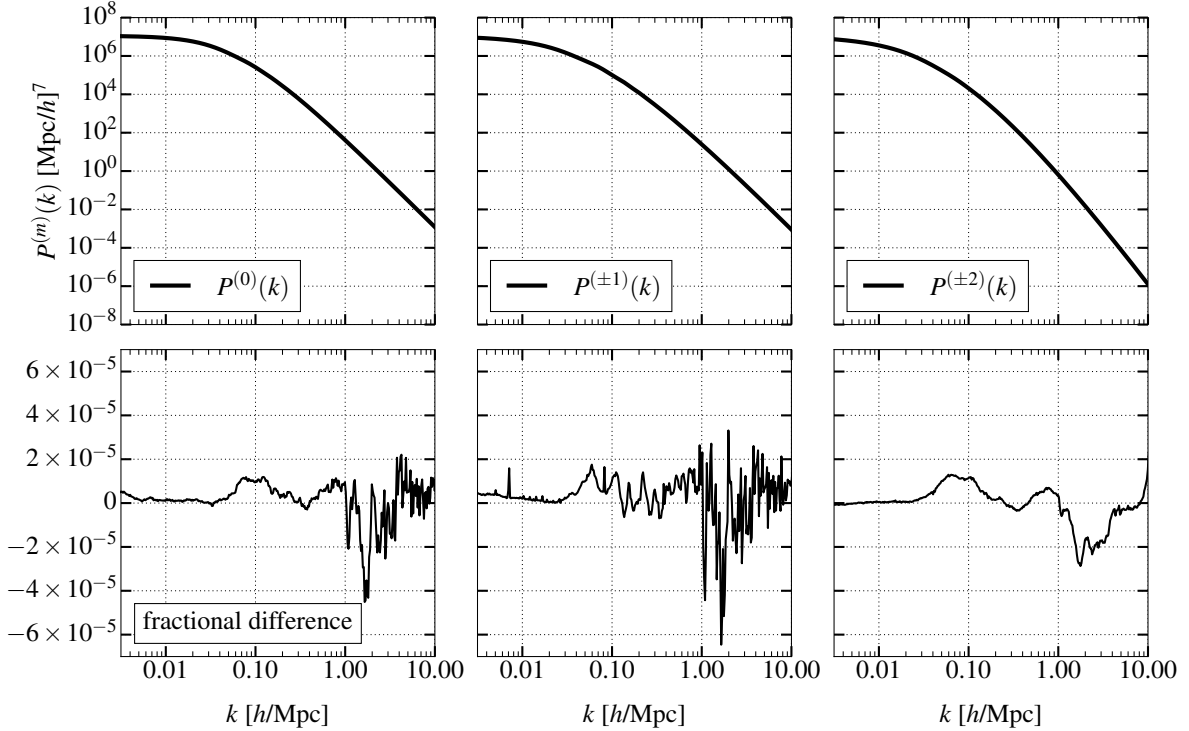


Figure 4. The FAST-PT results for the kinetic CMB polarization integrals $P^{(m)}(k)$ in Eq. (3.19) (upper panels) and the fractional difference compared to the conventional method (lower panels).

Tracers tend to infall towards overdense regions and, due to the Doppler effect, will thus have observed redshifts that deviate from those predicted by pure cosmological expansion. These deviations cause “redshift-space distortions” (RSDs) in the observed tracer distribution. Although at highly nonlinear scales RSDs are no longer well-described by perturbation theory, *e.g.* the “Fingers of God” (FoG) effect [67], we can still explore the mildly nonlinear regime via perturbation theory, avoiding time-consuming numerical simulations.

The “textbook” model for linear RSDs, the Kaiser effect [13], relates the matter power spectrum in redshift space matter to that in real space matter with an angular-dependent bias factor related to the growth rate of structure. Subsequently, [14] improved the Kaiser model by distinguishing $P_{\delta\theta}$ and $P_{\theta\theta}$ from $P_{\delta\delta}$, where θ is the divergence of velocity field. In the linear regime of standard perturbation theory, these three power spectra are equal to each other.

The TNS model [15] accounts for the nonlinear mode coupling between density and velocity fields, improving the modeling of the matter power spectrum in redshift space across a range of scales (including the BAO scale). Fixing \mathbf{k} along the \hat{z} direction, and defining θ_n as the angle between $\hat{\mathbf{n}}$ (the line-of-sight direction) and \mathbf{k} , with $\mu_n \equiv \cos \theta_n$, the density power spectrum in the redshift space can be written:

$$P^{(S)}(k, \mu_n) = D_{\text{FoG}}[k\mu_n f\sigma_v] \left\{ P_{\delta\delta}(k) + 2f\mu_n^2 P_{\delta\theta}(k) + f^2\mu_n^4 P_{\theta\theta}(k) + A(k, \mu_n) + B(k, \mu_n) \right\} , \quad (3.21)$$

where $D_{\text{FoG}}[k\mu_n f\sigma_v]$ encapsulates the contribution from the FoG effect. The A, B terms are

tensor convolution integrals given by

$$\bar{A}(k, \mu_n) \equiv \frac{A(k, \mu_n)}{k\mu_n f} = \int \frac{d^3 \mathbf{q}_1}{(2\pi)^3} \frac{q_{1n}}{q_1^2} [B_\sigma(\mathbf{q}_1, \mathbf{q}_2, -\mathbf{k}) - B_\sigma(\mathbf{q}_1, \mathbf{k}, -\mathbf{k} - \mathbf{q}_1)] , \quad (3.22)$$

$$\bar{B}(k, \mu_n) \equiv \frac{B(k, \mu_n)}{(k\mu_n f)^2} = \int \frac{d^3 \mathbf{q}_1}{(2\pi)^3} F(\mathbf{q}_1) F(\mathbf{q}_2) , \quad (3.23)$$

where $\mathbf{k} = \mathbf{q}_1 + \mathbf{q}_2$, and the subscript “ n ” denotes the projection onto $\hat{\mathbf{n}}$, *e.g.* $q_{1n} \equiv \mathbf{q}_1 \cdot \hat{\mathbf{n}}$, and

$$F(\mathbf{q}) = \frac{q_n}{q^2} \left(P_{\delta\theta}(q) + f \frac{q_n^2}{q^2} P_{\theta\theta}(q) \right) . \quad (3.24)$$

The cross bispectra B_σ is defined by

$$\left\langle \theta(\mathbf{k}_1) \left[\delta(\mathbf{k}_2) + f \frac{k_{2n}^2}{k_2^2} \theta(\mathbf{k}_2) \right] \left[\delta(\mathbf{k}_3) + f \frac{k_{3n}^2}{k_3^2} \theta(\mathbf{k}_3) \right] \right\rangle = (2\pi)^3 \delta_D(\mathbf{k}_1 + \mathbf{k}_2 + \mathbf{k}_3) B_\sigma(\mathbf{k}_1, \mathbf{k}_2, \mathbf{k}_3) . \quad (3.25)$$

The convolution integrals $\bar{A}(k, \mu_n)$ and $\bar{B}(k, \mu_n)$ are particularly time-consuming (*e.g.* [68]) and are ideal applications for our algorithm.

\bar{B} Term

Substituting the $F(\mathbf{q})$ kernel into the $\bar{B}(k, \mu_n)$ integral, we obtain

$$\begin{aligned} \bar{B}(k, \mu_n) &= \int \frac{d^3 \mathbf{q}_1}{(2\pi)^3} \frac{q_{1n} q_{2n}}{q_1^2 q_2^2} \left[P_{\delta\theta}(q_1) P_{\delta\theta}(q_2) + f^2 \frac{q_{1n}^2 q_{2n}^2}{q_1^2 q_2^2} P_{\theta\theta}(q_1) P_{\theta\theta}(q_2) + 2f \frac{q_{2n}^2}{q_2^2} P_{\delta\theta}(q_1) P_{\theta\theta}(q_2) \right] \\ &= \int \frac{d^3 \mathbf{q}_1}{(2\pi)^3} \frac{(\hat{\mathbf{q}}_1 \cdot \hat{\mathbf{n}})(\hat{\mathbf{q}}_2 \cdot \hat{\mathbf{n}})}{q_1 q_2} P_{\text{lin}}(q_1) P_{\text{lin}}(q_2) + f^2 \int \frac{d^3 \mathbf{q}_1}{(2\pi)^3} \frac{(\hat{\mathbf{q}}_1 \cdot \hat{\mathbf{n}})^3 (\hat{\mathbf{q}}_2 \cdot \hat{\mathbf{n}})^3}{q_1 q_2} P_{\text{lin}}(q_1) P_{\text{lin}}(q_2) \\ &\quad + 2f \int \frac{d^3 \mathbf{q}_1}{(2\pi)^3} \frac{(\hat{\mathbf{q}}_1 \cdot \hat{\mathbf{n}})(\hat{\mathbf{q}}_2 \cdot \hat{\mathbf{n}})^3}{q_1 q_2} P_{\text{lin}}(q_1) P_{\text{lin}}(q_2) . \end{aligned} \quad (3.26)$$

As previously mentioned, $P_{\delta\theta}, P_{\theta\theta}, P_{\delta\delta}$ are all equal to P_{lin} at the leading order. Since terms in the form of $(\hat{\mathbf{q}}_1 \cdot \hat{\mathbf{n}})^{p_1} (\hat{\mathbf{q}}_2 \cdot \hat{\mathbf{n}})^{p_2}$ with non-negative integers p_1, p_2 can always be decomposed as a polynomial in terms of $\hat{\mathbf{k}} \cdot \hat{\mathbf{n}}$ after longitude angle averaging (see Appendix C for a proof), it is natural to write \bar{B} as

$$\bar{B}(k, \mu_n) = \sum_{i=0} B_i(k) \mu_n^i , \quad (3.27)$$

where each $B_i(k)$ is a tensor convolution integral that can be written in terms of products of Legendre polynomials.

\bar{A} Term

The cross bispectrum satisfies $B_\sigma(\mathbf{k}_1, \mathbf{k}_2, \mathbf{k}_3) = B_\sigma(-\mathbf{k}_1, -\mathbf{k}_2, -\mathbf{k}_3) = B_\sigma(\mathbf{k}_1, \mathbf{k}_3, \mathbf{k}_2)$, so we can write the \bar{A} integral as

$$\bar{A}(k, \mu_n) = \int \frac{d^3 \mathbf{q}_1}{(2\pi)^3} \frac{q_{1n}}{q_1^2} [B_\sigma(\mathbf{q}_1, \mathbf{q}_2, -\mathbf{k}) - B_\sigma(-\mathbf{q}_1, \mathbf{k} + \mathbf{q}_1, -\mathbf{k})] . \quad (3.28)$$

Changing the dummy variable \mathbf{q}_1 to $-\mathbf{q}_1$ in the second term, we have

$$\bar{A}(k, \mu_n) = \int \frac{d^3 \mathbf{q}_1}{(2\pi)^3} \frac{q_{1n}}{q_1^2} [B_\sigma(\mathbf{q}_1, \mathbf{q}_2, -\mathbf{k}) + B_\sigma(\mathbf{q}_1, \mathbf{k} - \mathbf{q}_1, -\mathbf{k})] = 2 \int \frac{d^3 \mathbf{q}_1}{(2\pi)^3} \frac{q_{1n}}{q_1^2} B_\sigma(\mathbf{q}_1, \mathbf{q}_2, -\mathbf{k}) . \quad (3.29)$$

	ℓ	ℓ_1	ℓ_2	$A_{\ell_1 \ell_2 \ell}^{\alpha\beta}$			
				$i = 0$	$i = 2$	$i = 4$	$i = 6$
B_i	0	1	1	$-1/2 - 3f/10 - f^2/20$	$3/2 + 3f^2/20$	$3f/2 - 21f^2/20$	$131f^2/100$
		3	1	$3f/10 + f^2/10$	$-3f - 6f^2/5$	$7f/2 - 3f^2/10$	$47f^2/25$
		3	3	$-f^2/20$	$21f^2/20$	$-63f^2/20$	$231f^2/100$
	1	0	0	$(1+f)/2 + 5f^2/36$	$-1/2 + f^2/12$	$-f/2 - f^2/12$	$-5f^2/36$
		2	0	$-f/2 - 5f^2/18$	$3f + 4f^2/3$	$-5f/2 + f^2/6$	$-11f^2/9$
		2	2	$5f^2/36$	$-17f^2/12$	$53f^2/12$	$-113f^2/36$

Table 2. The coefficient of each term in the Legendre polynomial expansion of kernels of $B_i(k)$. $\alpha = \beta = -1$ for all the terms. Due to symmetry, we need only keep terms with $\ell_1 \geq \ell_2$ (multiplying the value by two where relevant). Empty entries are equal to the previous row.

Expanding the left-hand side of Eq. (3.25) to the leading order, we have

$$\begin{aligned}
B_\sigma(\mathbf{q}_1, \mathbf{q}_2, -\mathbf{k}) = & 2 \left(1 + \frac{q_{2n}^2}{q_2^2} f \right) \left(1 + \frac{k_n^2}{k^2} f \right) G_2(\mathbf{q}_2, -\mathbf{k}) P_{\text{lin}}(q_2) P_{\text{lin}}(k) \\
& + 2 \left(1 + \frac{k_n^2}{k^2} f \right) \left(F_2(\mathbf{q}_1, -\mathbf{k}) + \frac{q_{2n}^2}{q_2^2} f G_2(\mathbf{q}_1, -\mathbf{k}) \right) P_{\text{lin}}(q_1) P_{\text{lin}}(k) \\
& + 2 \left(1 + \frac{q_{2n}^2}{q_2^2} f \right) \left(F_2(\mathbf{q}_1, \mathbf{q}_2) + \frac{k_n^2}{k^2} f G_2(\mathbf{q}_1, \mathbf{q}_2) \right) P_{\text{lin}}(q_1) P_{\text{lin}}(q_2) . \quad (3.30)
\end{aligned}$$

Similarly, we can expand the integral \bar{A} as a polynomial in terms of μ_n :

$$\bar{A}(k, \mu_n) = \sum_{i=0} A_i(k) \mu_n^i . \quad (3.31)$$

Each $A_i(k)$ can be separated into two parts:

$$A_i(k) = A_i^{\text{I}}(k) + A_i^{\text{II}}(k) , \quad (3.32)$$

where $A_i^{\text{I}}(k)$ is a convolution integral with $P_{\text{lin}}(q_1)P_{\text{lin}}(q_2)$ in the integrand, while $A_i^{\text{II}}(k)$ has an integrand with $P_{\text{lin}}(q_1)P_{\text{lin}}(k)$ or $P_{\text{lin}}(q_2)P_{\text{lin}}(k)$, which is similar to the P_{13} integral and can be treated in a similar fashion.

3.4.2 Conversion to FAST-PT Format

The $B_i(k)$ and $A_i^{\text{I}}(k)$ integrals are standard convolution integrals, which can be decomposed into the form of Eq. (2.2). The associated coefficients $A_{\ell_1 \ell_2 \ell}^{\alpha\beta}$ are listed in Tables 2 and 3.

The $A_i^{\text{II}}(k)$ integrals are first decomposed into the form of

$$P_{\ell_1 \ell_2 \ell}^{\alpha\beta\gamma}(k) = \int \frac{d^3 \mathbf{q}_1}{(2\pi)^3} q_1^\alpha q_2^\beta k^\gamma \mathcal{P}_{\ell_1}(\hat{\mathbf{q}}_2 \cdot \hat{\mathbf{k}}) \mathcal{P}_{\ell_2}(\hat{\mathbf{q}}_1 \cdot \hat{\mathbf{k}}) \mathcal{P}_\ell(\hat{\mathbf{q}}_1 \cdot \hat{\mathbf{q}}_2) P_{\text{lin}}(q_1) P_{\text{lin}}(k) , \quad (3.33)$$

with coefficients $A_{\ell_1 \ell_2 \ell}^{\alpha\beta\gamma}$ given by Table 4, so that for each A_i^{II} integral,

$$A_i^{\text{II}}(k) = \sum A_{\ell_1 \ell_2 \ell}^{\alpha\beta\gamma} P_{\ell_1 \ell_2 \ell}^{\alpha\beta\gamma}(k) . \quad (3.34)$$

Note that for $P_{\text{lin}}(q_2)P_{\text{lin}}(k)$ terms one can always exchange the indices ($1 \leftrightarrow 2$) of q and ℓ in the integrand to recover the form above. For the special case that $\beta = \ell_1 = \ell = 0$ and $\ell_2 \neq 0$,

	α	β	ℓ	ℓ_1	ℓ_2	$A_{\ell_1 \ell_1 \ell}^{\alpha \beta}$		
						$i = 1$	$i = 3$	$i = 5$
A_i^I	-1	0	0	0	1	$68/21 + 2f/3$	$26f/9 + 2f^2/3$	$10f^2/63$
				2	1	$-68f/21$	$340f/63 - 52f^2/21$	$260f^2/63$
				1	1	$2 + 124f/35$	$-92f/105 + 108f^2/35$	$-254f^2/105$
				2	0	$-2f$	$10f/3 - 2f^2$	$10f^2/3$
				2	0	$16/21 + 4f/3$	$4f/9 + 4f^2/3$	$-52f^2/63$
				2	1	$-16f/21$	$80f/63 - 32f^2/21$	$160f^2/63$
	-2	1	0	1	0	$16f/35$	$-16f/35 + 32f^2/35$	$-32f^2/35$
				0	1	$2f/3$	$-2f/3 + 2f^2/3$	$-2f^2/3$
				1	0	2	$8f/3$	$2f^2/3$
				2	1	$-2f$	$10f/3 - 2f^2$	$10f^2/3$
				2	1	$4f/3$	$-4f/3 + 4f^2/3$	$-4f^2/3$
				2	1	$4f/3$	$-4f/3 + 4f^2/3$	$-4f^2/3$

Table 3. The coefficient of each term in the Legendre polynomial expansion of kernels of $A_i^I(k)$. The empty entries mean that they equal to the previous row.

the integral vanishes. These P_{13} -like integrals can be further reduced to one-dimensional integrals and quickly calculated using discrete convolutions as done for P_{13} in [46].

$$\begin{aligned}
P_{\ell_1 \ell_2 \ell}^{\alpha \beta \gamma}(k) &= k^\gamma P_{\text{lin}}(k) \int \frac{d^3 \mathbf{q}_1}{(2\pi)^3} q_1^\alpha q_2^\beta \mathcal{P}_{\ell_1} \left(\frac{k - q_1 \mu_2}{q_2} \right) \mathcal{P}_{\ell_2}(\mu_2) \mathcal{P}_\ell \left(\frac{k \mu_2 - q_1}{q_2} \right) P_{\text{lin}}(q_1) \\
&= \frac{k^\gamma P_{\text{lin}}(k)}{(2\pi)^2} \int_0^\infty dq_1 q_1^{2+\alpha} P_{\text{lin}}(q_1) \int_{-1}^1 d\mu_2 q_2^\beta \mathcal{P}_{\ell_1} \left(\frac{k - q_1 \mu_2}{q_2} \right) \mathcal{P}_{\ell_2}(\mu_2) \mathcal{P}_\ell \left(\frac{k \mu_2 - q_1}{q_2} \right), \tag{3.35}
\end{aligned}$$

where $q_2 = \sqrt{k^2 + q_1^2 - 2kq_1\mu_2}$. The angular (μ_2) integration can be performed analytically.¹¹ Summing the components, we find:

$$A_i^{\text{II}}(k) = \frac{k^2 P_{\text{lin}}(k)}{672\pi^2} \int_0^\infty dr P_{\text{lin}}(kr) Z_i(r), \quad i = 1, 3, 5, \tag{3.36}$$

where

$$\begin{aligned}
Z_1(r) &= \frac{18f}{r^2} - 152 - 66f + (192 - 66f)r^2 - (72 - 18f)r^4 \\
&+ \left[\frac{9f}{r^3} + \frac{36(1-f)}{r} - 54(2-f)r + 36(3-f)r^3 - 9(4-f)r^5 \right] \ln \left| \frac{1-r}{1+r} \right|, \tag{3.37}
\end{aligned}$$

$$\begin{aligned}
Z_3(r) &= \frac{18f(1+f)}{r^2} - 370f - 66f^2 + (318f - 66f^2)r^2 - (126f - 18f^2)r^4 \\
&+ \left[\frac{9f(1+f)}{r^3} + \frac{36f(1-f)}{r} - 54f(3-f)r + 36f(5-f)r^3 - 9f(7-f)r^5 \right] \ln \left| \frac{1-r}{1+r} \right|,
\end{aligned}$$

$$\begin{aligned}
Z_5(r) &= \frac{18f^2}{r^2} - 218f^2 + 126f^2r^2 - 54f^2r^4 + \left[\frac{9f^2}{r^3} - 54f^2r + 72f^2r^3 - 27f^2r^5 \right] \ln \left| \frac{1-r}{1+r} \right|.
\end{aligned}$$

¹¹There are several ways to do this; a brute-force approach is to write μ_2 in terms of q_2 (at fixed k and q_1), which turns the integral into a linear combination of power laws in q_2 .

The integral (3.36) is a convolution. Upon making the substitution $r = e^{-s}$, Eq. (3.36) becomes

$$\begin{aligned} A_i^{\text{II}}(k) &= \frac{k^2 P_{\text{lin}}(k)}{672\pi^2} \int_{-\infty}^{\infty} ds e^{-s} P_{\text{lin}}(e^{\log k - s}) Z_i(e^{-s}) \\ &= \frac{k^2 P_{\text{lin}}(k)}{672\pi^2} \int_{-\infty}^{\infty} ds G_i(s) F(\log k - s), \end{aligned} \quad (3.38)$$

where $G_i(s) \equiv e^{-s} Z_i(e^{-s})$ and $F(s) \equiv P_{\text{lin}}(e^s)$. We can convert to a discrete convolution with the substitutions $ds \rightarrow \Delta$, $\log k_n = \log k_0 + n\Delta$, and $s_m = \log k_0 + m\Delta$ (where k_0 is the smallest value in the k array):

$$\int_{-\infty}^{\infty} ds G_i(s) F(\log k - s) \rightarrow \Delta \sum_{m=0}^{N-1} G_i^D(m) F^D(n - m), \quad (3.39)$$

where in the final line we define the discrete functions $G_i^D(m) \equiv G_i(s_m)$ and $F^D(m) \equiv F(m\Delta)$. We then have

$$A_i^{\text{II}}(k_n) = \frac{k_n^2 P_{\text{lin}}(k_n) \Delta}{672\pi^2} [G_i^D \otimes F^D][n], \quad i = 1, 3, 5. \quad (3.40)$$

Thus $A_i^{\text{II}}(k)$, which at first appears to involve order N^2 steps (an integral over N samples at each of N output values k_n), can in fact be computed for all output k_n in $\mathcal{O}(N \log N)$ steps¹².

Note that some integrals $P_{\ell_1 \ell_2 \ell}^{\alpha \beta \gamma}(k)$ suffer from a divergence due to contributions from small-scales. When summing to get A_i^{II} , the divergent parts cancel each other precisely. Taking q_1 to be large, so that $\mathbf{q}_2 \rightarrow -\mathbf{q}_1$ and $P_{\text{lin}}(q_1) \propto q_1^{-3}$, we have

$$P_{\ell_1 \ell_2 \ell}^{\alpha \beta \gamma}(k) \rightarrow \frac{(-1)^{\ell + \ell_1} \delta_{\ell_1 \ell_2} k^\gamma P_{\text{lin}}(k)}{(2\ell_1 + 1) 2\pi^2} \int dq_1 q_1^{2 + \alpha + \beta} P_{\text{lin}}(q_1) \propto \int dq_1 q_1^{\alpha + \beta - 1}, \quad (3.41)$$

so that the divergence appears when $\ell_1 = \ell_2$ and $\alpha + \beta \geq 0$. In Table 4 there are 5 terms that suffer from this divergence problem. However these divergences cancel in A_i^{II} ; in our case, the cancellation occurs when doing the sum over $(\alpha, \beta, \gamma, \ell_1, \ell_2, \ell)$ to derive $Z_i(r)$.

In Figures 5, we show the FAST-PT results of $A + B$ terms in the TNS model (Eq. 3.21) for $f = 1$ and $\mu_n = 0.05, 0.5, 0.9$, respectively, as well as the fractional difference compared to our conventional method. The plots show excellent agreement between two methods with accuracy at the 10^{-4} level for most of the k range from 0.01 to 10 h/Mpc . Note that the individual A and B terms agree to significantly higher precision ($\sim 10^{-5}$). Cancellations among terms in the total $A + B$ amplify the fractional difference, especially at high k and near the zero-crossing.

4 Summary

In this paper we have extended the FAST-PT algorithm to treat 1-loop convolution integrals with tensor kernels (explicitly dependent on the direction of the observed mode). The generalized algorithm has many applications – we have presented quadratic intrinsic alignments, the

¹²In principle, N is the size of the input k array. However, to suppress the possible ringing and aliasing effects, we need to apply appropriate window functions, zero-padding or extend the input power spectrum into a larger range. The true value of N is usually a few times larger than the original value, depending on the user's inputs and options.

	γ	α	β	ℓ	ℓ_1	ℓ_2	$A_{\ell_1 \ell_1 \ell}^{\alpha \beta \gamma}$		
							$i = 1$	$i = 3$	$i = 5$
A_i^{II}	0	-1	0	0	2	1	$-108f/35$	$36f/7 - 108f^2/35$	$36f^2/7$
						3	$-32f/35$	$32f/21 - 32f^2/35$	$32f^2/21$
						1 1	0	$52f/21$	$-52f/21 + 52f^2/21$
				2	$32f/21$	$-32f/21 + 32f^2/21$	$-32f^2/21$		
				0 1	0	$52/21 - 32f/105$	$80f/21 - 32f^2/105$	$4f^2/3$	
				2	$32/21 - 428f/147$	$1012f/147 - 428f^2/147$	$788f^2/147$		
		4	$-192f/245$	$64f/49 - 192f^2/245$	$64f^2/49$				
		1 0	1	1	$108f/35$	$-108f/35 + 108f^2/35$	$-108f^2/35$		
		3	$32f/35$	$-32f/35 + 32f^2/35$	$-32f^2/35$				
		0 0	0	0	0	$-2/3$	$-8f/9$	$-2f^2/9$	
		2 0	0	0	0	$2f/3$	$-10f/9 + 2f^2/3$	$-10f^2/9$	
		2	0	0	0	$4f/3$	$-20f/9 + 4f^2/3$	$-20f^2/9$	
	1 1	1	1	1	$-2f$	$2f - 2f^2$	$2f^2$		
	0 1	1	-1	0	1	$-2 + 4f/5$	$-4f + 4f^2/5$	$-2f^2$	
	3	$6f/5$	$-2f + 6f^2/5$	$-2f^2$					
	1 0	0	0	0	$-2f/3$	$2f/3 - 2f^2/3$	$2f^2/3$		
	2	$-4f/3$	$4f/3 - 4f^2/3$	$4f^2/3$					
	0 0	1	-2	0	0	0	$-2/3$	$-8f/9$	$-2f^2/9$
	2 0	0	0	0	0	0	$2f/3$	$-10f/9 + 2f^2/3$	$-10f^2/9$
	2	0	0	0	0	0	$4f/3$	$-20f/9 + 4f^2/3$	$-20f^2/9$
	1 1	1	1	1	1	1	$-2f$	$2f - 2f^2$	$2f^2$
	0 1	-1	-1	0	1	1	$-2 + 4f/5$	$-4f + 4f^2/5$	$-2f^2$
	3	$6f/5$	$-2f + 6f^2/5$	$-2f^2$					
	1 0	0	0	0	0	0	$-2f/3$	$2f/3 - 2f^2/3$	$2f^2/3$
2	$-4f/3$	$4f/3 - 4f^2/3$	$4f^2/3$						

Table 4. The coefficient of each term in the Legendre polynomial expansion of kernels of $A_i^{\text{II}}(k)$.

Ostriker-Vishniac effect, kinetic CMB polarizations, and a sophisticated model for redshift space distortions. Our algorithm and code achieve high precision for all of these applications. We have tested the output of the code to high wavenumber ($k = 10 h/\text{Mpc}$), although we reiterate that the smaller scales considered are beyond the range of validity of the underlying perturbative models. The reduction in evaluation time is similar as for the scalar FAST-PT. For instance, execution time is ~ 0.1 seconds for 600 k values in all our examples. In the results shown here, the input power spectrum was sampled at 100 points per \log_{10} interval. We find that much of the noise (in comparisons with the conventional method) is driven by the exact process by which the CAMB power spectrum is interpolated before it is used in FAST-PT.

There are underlying physical concepts and symmetries that make the efficiency of this algorithm possible. For example, the locality of the gravitational interactions allows us to separate different modes in configuration space. Since the structure evolution under gravity only depends on the local density and velocity divergence fields, in Fourier space the 1-loop power spectra of the matter density as well as its tracers (assuming local biasing theories) must be in form of Eq. (1.1), where the kernels can always be written in terms of dot products of different mode vectors. Without this locality, it may not be possible to write the desired

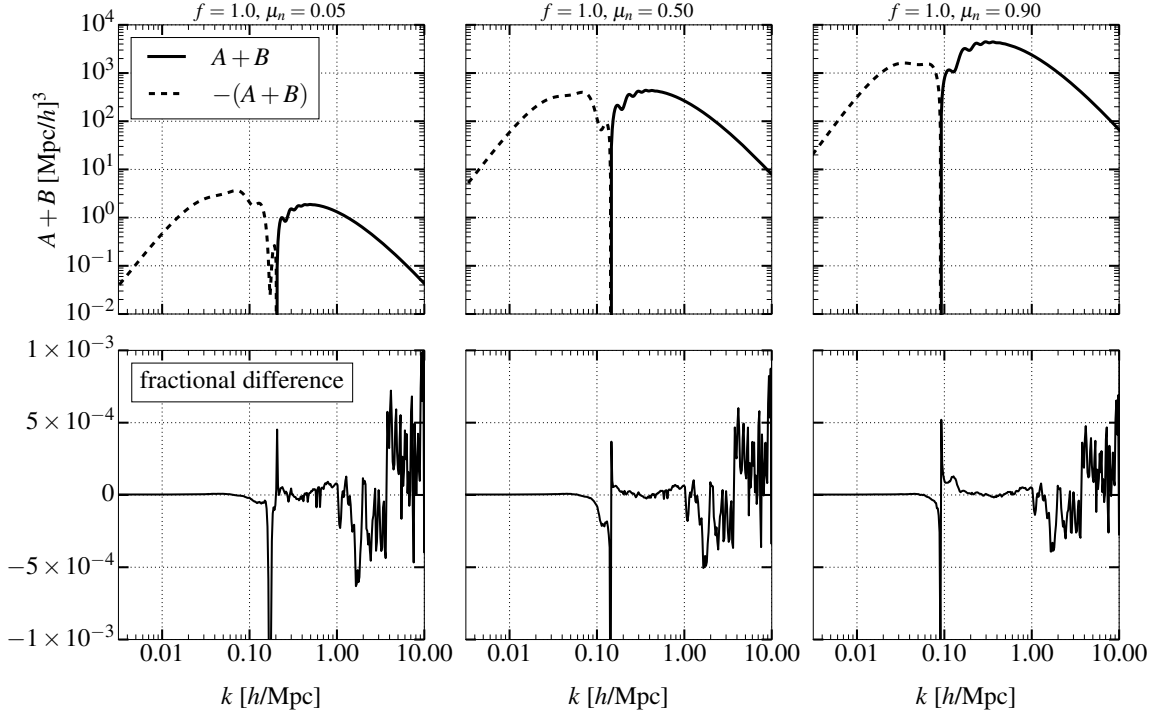


Figure 5. The FAST-PT result for the redshift space distortion nonlinear corrections $A(k, \mu_n) + B(k, \mu_n)$ in the TNS model, Eq. (3.21) (upper panels) and the fractional difference compared to the conventional method result (lower panels).

power spectrum as a sum of terms that can be calculated with this algorithm. The scale invariance of the problem also indicates that we should decompose the input power spectrum into a set of power-law spectra and make full use of the FFT algorithm. There are also rotational symmetries that allow us to reduce the 3-dimensional integrals to 1-dimension.

This algorithm, and implementations of the examples presented here, are publicly available as a Python code package at <https://github.com/JoeMcEwen/FAST-PT>.

Acknowledgments

XF is supported by the Simons Foundation, JB is supported by a CCAPP Fellowship, JM is supported by NSF grant AST1516997, and CH by the Simons Foundation, the US Department of Energy, the Packard Foundation, and NASA.

References

- [1] DESI collaboration, M. Levi et al., *The DESI Experiment, a whitepaper for Snowmass 2013*, [1308.0847](#).
- [2] K. S. Dawson, D. J. Schlegel, C. P. Ahn, S. F. Anderson, É. Aubourg, S. Bailey et al., *The Baryon Oscillation Spectroscopic Survey of SDSS-III*, *Astron. J.* **145** (2013) 10, [[1208.0022](#)].
- [3] R. Laureijs, J. Amiaux, S. Arduini, J. . Auguères, J. Brinchmann, R. Cole et al., *Euclid Definition Study Report, ArXiv e-prints* (Oct., 2011) , [[1110.3193](#)].

- [4] D. Spergel, N. Gehrels, J. Breckinridge, M. Donahue, A. Dressler, B. S. Gaudi et al., *Wide-Field InfraRed Survey Telescope-Astrophysics Focused Telescope Assets WFIRST-AFTA Final Report, ArXiv e-prints* (2013) , [[1305.5422](#)].
- [5] DES collaboration, T. Abbott et al., *The Dark Energy Survey: more than dark energy - an overview*, *Mon. Not. Roy. Astron. Soc.* (2016) , [[1601.00329](#)].
- [6] M. Bartelmann and P. Schneider, *Weak gravitational lensing*, *Phys. Rept.* **340** (2001) 291–472, [[astro-ph/9912508](#)].
- [7] Y. Mellier, *Probing the universe with weak lensing*, *Ann. Rev. Astron. Astrophys.* **37** (1999) 127–189, [[astro-ph/9812172](#)].
- [8] SDSS collaboration, U. Seljak, A. Makarov, R. Mandelbaum, C. M. Hirata, N. Padmanabhan, P. McDonald et al., *SDSS galaxy bias from halo mass-bias relation and its cosmological implications*, *Phys. Rev.* **D71** (2005) 043511, [[astro-ph/0406594](#)].
- [9] P. McDonald, *Clustering of dark matter tracers: Renormalizing the bias parameters*, *Phys. Rev.* **D74** (2006) 103512, [[astro-ph/0609413](#)].
- [10] P. McDonald and A. Roy, *Clustering of dark matter tracers: generalizing bias for the coming era of precision LSS*, *J. Cosmo. Astropart. Phys.* **8** (Aug., 2009) 020, [[0902.0991](#)].
- [11] T. Baldauf, U. Seljak, L. Senatore and M. Zaldarriaga, *Galaxy Bias and non-Linear Structure Formation in General Relativity*, *JCAP* **1110** (2011) 031, [[1106.5507](#)].
- [12] U. Seljak, *Bias, redshift space distortions and primordial nongaussianity of nonlinear transformations: application to Ly- α forest*, *J. Cosmo. Astropart. Phys.* **3** (Mar., 2012) 004, [[1201.0594](#)].
- [13] N. Kaiser, *Clustering in real space and in redshift space*, *Mon. Not. R. Astron. Soc.* **227** (1987) 1–21.
- [14] R. Scoccimarro, *Redshift-space distortions, pairwise velocities and nonlinearities*, *Phys. Rev.* **D70** (2004) 083007, [[astro-ph/0407214](#)].
- [15] A. Taruya, T. Nishimichi and S. Saito, *Baryon Acoustic Oscillations in 2D: Modeling Redshift-space Power Spectrum from Perturbation Theory*, *Phys. Rev.* **D82** (2010) 063522, [[1006.0699](#)].
- [16] I. A. Strukov, A. A. Brukhanov, D. P. Skulachev and M. V. Sazhin, *Anisotropy of the microwave background radiation*, *Soviet Astronomy Letters* **18** (1992) 153.
- [17] G. F. Smoot, C. Bennett, A. Kogut, E. Wright, J. Aymon et al., *Structure in the COBE differential microwave radiometer first year maps*, *Astrophys.J.* **396** (1992) L1–L5.
- [18] J. Kovac, E. Leitch, C. Pryke, J. Carlstrom, N. Halverson et al., *Detection of polarization in the cosmic microwave background using DASI*, *Nature* **420** (2002) 772–787, [[astro-ph/0209478](#)].
- [19] A. Readhead, S. Myers, T. J. Pearson, J. Sievers, B. Mason et al., *Polarization observations with the Cosmic Background Imager*, *Science* **306** (2004) 836, [[astro-ph/0409569](#)].
- [20] WMAP collaboration, C. Bennett et al., *Nine-Year Wilkinson Microwave Anisotropy Probe (WMAP) Observations: Final Maps and Results*, *Astrophys.J.Suppl.* **208** (2013) 20, [[1212.5225](#)].
- [21] SPT collaboration, A. T. Crites et al., *Measurements of E-Mode Polarization and Temperature-E-Mode Correlation in the Cosmic Microwave Background from 100 Square Degrees of SPTpol Data*, *Astrophys. J.* **805** (2015) 36, [[1411.1042](#)].
- [22] ACTPOL collaboration, S. Naess et al., *The Atacama Cosmology Telescope: CMB Polarization at $200 < \ell < 9000$* , *JCAP* **1410** (2014) 007, [[1405.5524](#)].

- [23] POLARBEAR collaboration, P. A. R. Ade et al., *Evidence for Gravitational Lensing of the Cosmic Microwave Background Polarization from Cross-correlation with the Cosmic Infrared Background*, *Phys. Rev. Lett.* **112** (2014) 131302, [[1312.6645](#)].
- [24] BICEP2, PLANCK collaboration, P. A. R. Ade et al., *Joint Analysis of BICEP2/KeckArray and Planck Data*, *Phys. Rev. Lett.* **114** (2015) 101301, [[1502.00612](#)].
- [25] PLANCK collaboration, R. Adam et al., *Planck 2015 results. I. Overview of products and scientific results*, [1502.01582](#).
- [26] A. Kogut, D. J. Fixsen, D. T. Chuss, J. Dotson, E. Dwek, M. Halpern et al., *The Primordial Inflation Explorer (PIXIE): a nulling polarimeter for cosmic microwave background observations*, *J. Cosmo. Astropart. Phys.* **7** (2011) 025, [[1105.2044](#)].
- [27] J. Bock, A. Aljabri, A. Amblard, D. Baumann, M. Betoule, T. Chui et al., *Study of the Experimental Probe of Inflationary Cosmology (EPIC)-Intermediate Mission for NASA's Einstein Inflation Probe*, *ArXiv e-prints* (2009) , [[0906.1188](#)].
- [28] J. Lazear, P. A. R. Ade, D. Benford, C. L. Bennett, D. T. Chuss, J. L. Dotson et al., *The Primordial Inflation Polarization Explorer (PIPER)*, in *Millimeter, Submillimeter, and Far-Infrared Detectors and Instrumentation for Astronomy VII*, vol. 9153, p. 91531L, 2014. [1407.2584](#). DOI.
- [29] PRISM collaboration, P. Andre et al., *PRISM (Polarized Radiation Imaging and Spectroscopy Mission): A White Paper on the Ultimate Polarimetric Spectro-Imaging of the Microwave and Far-Infrared Sky*, [1306.2259](#).
- [30] PRISM collaboration, P. Andre et al., *PRISM (Polarized Radiation Imaging and Spectroscopy Mission): An Extended White Paper*, *JCAP* **1402** (2014) 006, [[1310.1554](#)].
- [31] R. A. Sunyaev and Y. B. Zeldovich, *The Observations of Relic Radiation as a Test of the Nature of X-Ray Radiation from the Clusters of Galaxies*, *Comments on Astrophysics and Space Physics* **4** (Nov., 1972) 173.
- [32] J. E. Carlstrom, G. P. Holder and E. D. Reese, *Cosmology with the Sunyaev-Zel'dovich effect*, *Ann. Rev. Astron. Astrophys.* **40** (2002) 643–680, [[astro-ph/0208192](#)].
- [33] J. Chluba and R. A. Sunyaev, *The evolution of CMB spectral distortions in the early Universe*, *Mon. Not. Roy. Astron. Soc.* **419** (2012) 1294–1314, [[1109.6552](#)].
- [34] R. Khatri and R. A. Sunyaev, *Beyond y and μ : the shape of the CMB spectral distortions in the intermediate epoch, $1.5 \times 10^4 \lesssim z \lesssim 2 \times 10^5$* , *JCAP* **1209** (2012) 016, [[1207.6654](#)].
- [35] F. Bernardeau, S. Colombi, E. Gaztanaga and R. Scoccimarro, *Large scale structure of the universe and cosmological perturbation theory*, *Phys. Rept.* **367** (2002) 1–248, [[astro-ph/0112551](#)].
- [36] N. S. Sugiyama, *Using Lagrangian perturbation theory for precision cosmology*, *Astrophys. J.* **788** (2014) 63, [[1311.0725](#)].
- [37] M. Crocce and R. Scoccimarro, *Renormalized cosmological perturbation theory*, *Phys. Rev.* **D73** (2006) 063519, [[astro-ph/0509418](#)].
- [38] P. McDonald, *Dark matter clustering: a simple renormalization group approach*, *Phys. Rev.* **D75** (2007) 043514, [[astro-ph/0606028](#)].
- [39] P. McDonald, *What the "simple renormalization group" approach to dark matter clustering really was*, [1403.7235](#).
- [40] B. Audren and J. Lesgourgues, *Non-linear matter power spectrum from Time Renormalisation Group: efficient computation and comparison with one-loop*, *J. Cosmo. Astropart. Phys.* **10** (2011) 037, [[1106.2607](#)].

- [41] D. Baumann, A. Nicolis, L. Senatore and M. Zaldarriaga, *Cosmological Non-Linearities as an Effective Fluid*, *JCAP* **1207** (2012) 051, [[1004.2488](#)].
- [42] J. J. M. Carrasco, M. P. Hertzberg and L. Senatore, *The Effective Field Theory of Cosmological Large Scale Structures*, *JHEP* **09** (2012) 082, [[1206.2926](#)].
- [43] E. Pajer and M. Zaldarriaga, *On the Renormalization of the Effective Field Theory of Large Scale Structures*, *JCAP* **1308** (2013) 037, [[1301.7182](#)].
- [44] M. P. Hertzberg, *Effective field theory of dark matter and structure formation: Semianalytical results*, *Phys. Rev.* **D89** (2014) 043521, [[1208.0839](#)].
- [45] D. Blas, M. Garny, M. M. Ivanov and S. Sibiryakov, *Time-Sliced Perturbation Theory for Large Scale Structure I: General Formalism*, *JCAP* **1607** (2016) 052, [[1512.05807](#)].
- [46] J. E. McEwen, X. Fang, C. M. Hirata and J. A. Blazek, *FAST-PT: a novel algorithm to calculate convolution integrals in cosmological perturbation theory*, *JCAP* **1609** (2016) 015, [[1603.04826](#)].
- [47] M. Schmittfull, Z. Vlah and P. McDonald, *Fast large scale structure perturbation theory using one-dimensional fast Fourier transforms*, *Phys. Rev.* **D93** (2016) 103528, [[1603.04405](#)].
- [48] M. Schmittfull and Z. Vlah, *FFT-PT: Reducing the 2-loop large-scale structure power spectrum to one-dimensional, radial integrals*, [1609.00349](#).
- [49] E. Jones, T. Oliphant, P. Peterson et al., *SciPy: Open source scientific tools for Python*, 2001–.
- [50] A. Lewis, A. Challinor and A. Lasenby, *Efficient computation of CMB anisotropies in closed FRW models*, *Astrophys. J.* **538** (2000) 473–476, [[astro-ph/9911177](#)].
- [51] PLANCK collaboration, P. A. R. Ade et al., *Planck 2015 results. XIII. Cosmological parameters*, [1502.01589](#).
- [52] H. Hildebrandt et al., *KiDS-450: Cosmological parameter constraints from tomographic weak gravitational lensing*, [1606.05338](#).
- [53] M. A. Troxel and M. Ishak, *The Intrinsic Alignment of Galaxies and its Impact on Weak Gravitational Lensing in an Era of Precision Cosmology*, *Phys. Rept.* **558** (2014) 1–59, [[1407.6990](#)].
- [54] B. Joachimi et al., *Galaxy alignments: An overview*, *Space Sci. Rev.* **193** (2015) 1–65, [[1504.05456](#)].
- [55] E. Krause, T. Eifler and J. Blazek, *The impact of intrinsic alignment on current and future cosmic shear surveys*, *Mon. Not. Roy. Astron. Soc.* **456** (2016) 207–222, [[1506.08730](#)].
- [56] N. E. Chisari and C. Dvorkin, *Cosmological Information in the Intrinsic Alignments of Luminous Red Galaxies*, *JCAP* **1312** (2013) 029, [[1308.5972](#)].
- [57] C. M. Hirata and U. Seljak, *Intrinsic alignment-lensing interference as a contaminant of cosmic shear*, *Phys. Rev.* **D70** (2004) 063526, [[astro-ph/0406275](#)].
- [58] P. Catelan, M. Kamionkowski and R. D. Blandford, *Intrinsic and extrinsic galaxy alignment*, *Mon. Not. Roy. Astron. Soc.* **320** (2001) L7–L13, [[astro-ph/0005470](#)].
- [59] J. Blazek, Z. Vlah and U. Seljak, *Tidal alignment of galaxies*, *JCAP* **1508** (2015) 015, [[1504.02510](#)].
- [60] J. Blazek, M. Troxel and N. MacCrann, *Intrinsic Alignment Modeling for Mixed Galaxy Populations, in preparation*.
- [61] P. McDonald and A. Roy, *Clustering of dark matter tracers: generalizing bias for the coming era of precision LSS*, *J. Cosmo. Astropart. Phys.* **8** (2009) 020, [[0902.0991](#)].

- [62] J. P. Ostriker and E. T. Vishniac, *Generation of microwave background fluctuations from nonlinear perturbations at the ERA of galaxy formation*, *Astrophys. J. Lett.* **306** (1986) L51–L54.
- [63] E. T. Vishniac, *Reionization and small-scale fluctuations in the microwave background*, *Astrophys. J.* **322** (1987) 597–604.
- [64] A. H. Jaffe and M. Kamionkowski, *Calculation of the Ostriker-Vishniac effect in cold dark matter models*, *Phys. Rev.* **D58** (1998) 043001, [[astro-ph/9801022](#)].
- [65] R. A. Sunyaev and I. B. Zeldovich, *The velocity of clusters of galaxies relative to the microwave background - The possibility of its measurement*, *Mon. Not. R. Astron. Soc.* **190** (1980) 413–420.
- [66] W. Hu, *Reionization revisited: secondary cmb anisotropies and polarization*, *Astrophys. J.* **529** (2000) 12, [[astro-ph/9907103](#)].
- [67] J. C. Jackson, *Fingers of God: A critique of Rees’ theory of primordial gravitational radiation*, *Mon. Not. Roy. Astron. Soc.* **156** (1972) 1P–5P, [[0810.3908](#)].
- [68] B. Bose and K. Koyama, *A Perturbative Approach to the Redshift Space Power Spectrum: Beyond the Standard Model*, [1606.02520](#).
- [69] M. Abramowitz and I. A. Stegun, *Handbook of mathematical functions: with formulas, graphs, and mathematical tables*. No. 55. Courier Corporation, 1964.
- [70] “NIST Digital Library of Mathematical Functions.” <http://dlmf.nist.gov/>, Release 1.0.10 of 2015-08-07.
- [71] F. W. J. Olver, D. W. Lozier, R. F. Boisvert and C. W. Clark, eds., *NIST Handbook of Mathematical Functions*. Cambridge University Press, New York, NY, 2010.

A Mathematical Identities

In this work we have used a number of common mathematical identities. These identities are easily found in any standard mathematical physics text or handbook, (e.g. [69–71]). However, to make our paper self-contained we list those relevant to our paper.

A.1 Spherical Harmonics and Legendre Polynomials

- The addition theorem

$$P_\ell(\hat{\mathbf{q}}_1 \cdot \hat{\mathbf{q}}_2) = \frac{4\pi}{2\ell + 1} \sum_{m=-\ell}^{\ell} Y_{\ell m}(\hat{\mathbf{q}}_1) Y_{\ell m}^*(\hat{\mathbf{q}}_2); \quad (\text{A.1})$$

- The special case thereof,

$$\sum_{m=-\ell}^{\ell} Y_{\ell m}(\hat{\mathbf{q}}) Y_{\ell m}^*(\hat{\mathbf{q}}) = \frac{2\ell + 1}{4\pi}; \quad (\text{A.2})$$

- The orthonormality relation

$$\int_{S^2} d^2\hat{\mathbf{q}} Y_{\ell m}(\hat{\mathbf{q}}) Y_{\ell' m'}^*(\hat{\mathbf{q}}) = \delta_{\ell\ell'} \delta_{mm'}; \quad (\text{A.3})$$

- The symmetry

$$Y_{\ell m}(\hat{\mathbf{q}}) = (-1)^m Y_{\ell, -m}^*(\hat{\mathbf{q}}); \quad (\text{A.4})$$

- The expansion/decomposition of a plane wave:

$$\int_{S^2} d^2\hat{\mathbf{q}} Y_{\ell m}^*(\hat{\mathbf{q}}) e^{i\mathbf{q}\cdot\mathbf{r}} = 4\pi i^\ell j_\ell(qr) Y_{\ell m}^*(\hat{\mathbf{r}}) \quad \leftrightarrow \quad e^{i\mathbf{q}\cdot\mathbf{r}} = 4\pi \sum_{\ell} i^\ell j_\ell(qr) \sum_{m=-\ell}^{\ell} Y_{\ell m}^*(\hat{\mathbf{q}}) Y_{\ell m}(\hat{\mathbf{r}}). \quad (\text{A.5})$$

A.2 Wigner $3j$ and $6j$ Symbols

The definitions of Wigner $3j$ and $6j$ symbols, denoted by $\begin{pmatrix} \cdot & \cdot & \cdot \\ 0 & 0 & 0 \end{pmatrix}$ and $\{ \}$, respectively, are long and can be easily found online or in handbooks. Here we only list some properties and identities needed in our derivations.

- Assuming j_1, j_2, j_3 satisfy the triangle conditions, we have the special case

$$\begin{pmatrix} j_1 & j_2 & j_3 \\ 0 & 0 & 0 \end{pmatrix} = \begin{cases} 0, & J \text{ odd,} \\ (-1)^{J/2} \left(\frac{(J-2j_1)! (J-2j_2)! (J-2j_3)!}{(J+1)!} \right)^{1/2} \frac{(\frac{1}{2}J)!}{(\frac{1}{2}J-j_1)! (\frac{1}{2}J-j_2)! (\frac{1}{2}J-j_3)!}, & J \text{ even,} \end{cases} \quad (\text{A.6})$$

where $J \equiv j_1 + j_2 + j_3$;

- The permutation and reflection symmetry

$$\begin{pmatrix} j_1 & j_2 & j_3 \\ m_1 & m_2 & m_3 \end{pmatrix} = \begin{pmatrix} j_2 & j_3 & j_1 \\ m_2 & m_3 & m_1 \end{pmatrix} = \begin{pmatrix} j_3 & j_1 & j_2 \\ m_3 & m_1 & m_2 \end{pmatrix}, \quad (\text{A.7})$$

$$\begin{pmatrix} j_1 & j_2 & j_3 \\ m_1 & m_2 & m_3 \end{pmatrix} = (-1)^{j_1+j_2+j_3} \begin{pmatrix} j_2 & j_1 & j_3 \\ m_2 & m_1 & m_3 \end{pmatrix}; \quad (\text{A.7})$$

$$\begin{pmatrix} j_1 & j_2 & j_3 \\ m_1 & m_2 & m_3 \end{pmatrix} = (-1)^{j_1+j_2+j_3} \begin{pmatrix} j_1 & j_2 & j_3 \\ -m_1 & -m_2 & -m_3 \end{pmatrix}; \quad (\text{A.8})$$

- The orthogonality relation

$$\sum_{m_1 m_2} (2j_3 + 1) \begin{pmatrix} j_1 & j_2 & j_3 \\ m_1 & m_2 & m_3 \end{pmatrix} \begin{pmatrix} j_1 & j_2 & j_3' \\ m_1 & m_2 & m_3' \end{pmatrix} = \delta_{j_3, j_3'} \delta_{m_3, m_3'}, \quad (\text{A.9})$$

- Relation to spherical harmonics

$$Y_{\ell_1 m_1}(\hat{\mathbf{q}}) Y_{\ell_2 m_2}(\hat{\mathbf{q}}) = \sum_{\ell, m} \sqrt{\frac{(2\ell_1 + 1)(2\ell_2 + 1)(2\ell + 1)}{4\pi}} \begin{pmatrix} \ell_1 & \ell_2 & \ell \\ m_1 & m_2 & m \end{pmatrix} Y_{\ell m}^*(\hat{\mathbf{q}}) \begin{pmatrix} \ell_1 & \ell_2 & \ell \\ 0 & 0 & 0 \end{pmatrix}; \quad (\text{A.10})$$

$$\int d^2\hat{\mathbf{q}} Y_{\ell_1 m_1}(\hat{\mathbf{q}}) Y_{\ell_2 m_2}(\hat{\mathbf{q}}) Y_{\ell_3 m_3}(\hat{\mathbf{q}}) = \sqrt{\frac{(2\ell_1 + 1)(2\ell_2 + 1)(2\ell_3 + 1)}{4\pi}} \begin{pmatrix} \ell_1 & \ell_2 & \ell_3 \\ 0 & 0 & 0 \end{pmatrix} \begin{pmatrix} \ell_1 & \ell_2 & \ell_3 \\ m_1 & m_2 & m_3 \end{pmatrix}; \quad (\text{A.11})$$

$$\begin{aligned}
\begin{pmatrix} j_1 & j_2 & j_3 \\ m_1 & m_2 & m_3 \end{pmatrix} \begin{Bmatrix} j_1 & j_2 & j_3 \\ \ell_1 & \ell_2 & \ell_3 \end{Bmatrix} &= \sum_{m'_1 m'_2 m'_3} (-1)^{\ell_1 + \ell_2 + \ell_3 + m'_1 + m'_2 + m'_3} \\
&\times \begin{pmatrix} j_1 & \ell_2 & \ell_3 \\ m_1 & m'_2 & -m'_3 \end{pmatrix} \begin{pmatrix} \ell_1 & j_2 & \ell_3 \\ -m'_1 & m_2 & m'_3 \end{pmatrix} \begin{pmatrix} \ell_1 & \ell_2 & j_3 \\ m'_1 & -m'_2 & m_3 \end{pmatrix}.
\end{aligned} \tag{A.12}$$

B Derivations

B.1 Derivation of Eq. (2.3)

Applying identities (A.1, A.4, A.7, A.8, A.10, A.12), we obtain

$$\begin{aligned}
&\mathcal{P}_\ell(\hat{\mathbf{q}}_1 \cdot \hat{\mathbf{q}}_2) \mathcal{P}_{\ell_2}(\hat{\mathbf{q}}_1 \cdot \hat{\mathbf{k}}) \mathcal{P}_{\ell_1}(\hat{\mathbf{q}}_2 \cdot \hat{\mathbf{k}}) \\
&= \frac{(4\pi)^3}{(2\ell+1)(2\ell_1+1)(2\ell_2+1)} \sum_{m, m_1, m_2} (-1)^{m+m_1+m_2} \\
&\quad \times Y_{\ell m}(\hat{\mathbf{q}}_1) Y_{\ell, -m}(\hat{\mathbf{q}}_2) Y_{\ell_2 m_2}(\hat{\mathbf{q}}_1) Y_{\ell_2, -m_2}(\hat{\mathbf{k}}) Y_{\ell_1 m_1}(\hat{\mathbf{q}}_2) Y_{\ell_1, -m_1}(\hat{\mathbf{k}}) \\
&= (4\pi)^{\frac{3}{2}} \sum_{J_1, J_2, J_k} \sqrt{(2J_1+1)(2J_2+1)(2J_k+1)} \begin{pmatrix} \ell & \ell_2 & J_1 \\ 0 & 0 & 0 \end{pmatrix} \begin{pmatrix} \ell & \ell_1 & J_2 \\ 0 & 0 & 0 \end{pmatrix} \begin{pmatrix} \ell_2 & \ell_1 & J_k \\ 0 & 0 & 0 \end{pmatrix} \\
&\quad \times \sum_{M_1, M_2, M_k} (-1)^{M_1+M_2+M_k} Y_{J_1 M_1}(\hat{\mathbf{q}}_1) Y_{J_2 M_2}(\hat{\mathbf{q}}_2) Y_{J_k M_k}(\hat{\mathbf{k}}) \\
&\quad \times \sum_{m, m_1, m_2} (-1)^{m+m_1+m_2} \begin{pmatrix} \ell & \ell_2 & J_1 \\ m & m_2 & -M_1 \end{pmatrix} \begin{pmatrix} \ell & \ell_1 & J_2 \\ -m & m_1 & -M_2 \end{pmatrix} \begin{pmatrix} \ell_2 & \ell_1 & J_k \\ -m_2 & -m_1 & -M_k \end{pmatrix} \\
&= (4\pi)^{3/2} (-1)^{\ell_1 + \ell_2 + \ell} \\
&\quad \times \sum_{J_1, J_2, J_k} \sqrt{(2J_1+1)(2J_2+1)(2J_k+1)} \begin{pmatrix} J_1 & \ell_2 & \ell \\ 0 & 0 & 0 \end{pmatrix} \begin{pmatrix} \ell_1 & J_2 & \ell \\ 0 & 0 & 0 \end{pmatrix} \begin{pmatrix} \ell_1 & \ell_2 & J_k \\ 0 & 0 & 0 \end{pmatrix} \begin{Bmatrix} J_1 & J_2 & J_k \\ \ell_1 & \ell_2 & \ell \end{Bmatrix} \\
&\quad \times (-1)^{J_1+J_2+J_k} \sum_{M_1, M_2, M_k} Y_{J_1 M_1}(\hat{\mathbf{q}}_1) Y_{J_2 M_2}(\hat{\mathbf{q}}_2) Y_{J_k M_k}(\hat{\mathbf{k}}) \begin{pmatrix} J_1 & J_2 & J_k \\ M_1 & M_2 & M_k \end{pmatrix}, \tag{B.1}
\end{aligned}$$

where we can define a coefficient

$$\begin{aligned}
C_{\ell_1 \ell_2 \ell}^{J_1 J_2 J_k} &\equiv (4\pi)^{3/2} (-1)^{\ell_1 + \ell_2 + \ell + J_1 + J_2 + J_k} \\
&\quad \times \sqrt{(2J_1+1)(2J_2+1)(2J_k+1)} \begin{pmatrix} J_1 & \ell_2 & \ell \\ 0 & 0 & 0 \end{pmatrix} \begin{pmatrix} \ell_1 & J_2 & \ell \\ 0 & 0 & 0 \end{pmatrix} \begin{pmatrix} \ell_1 & \ell_2 & J_k \\ 0 & 0 & 0 \end{pmatrix} \begin{Bmatrix} J_1 & J_2 & J_k \\ \ell_1 & \ell_2 & \ell \end{Bmatrix}, \tag{B.2}
\end{aligned}$$

Note that when we combine two spherical harmonics into one, the triangle conditions of the $3j$ symbols imply that

$$M_1 = m + m_2, \quad M_2 = -m + m_1, \quad M_k = -m_1 - m_2, \tag{B.3}$$

so that M_1, M_2, M_k satisfy

$$M_1 + M_2 + M_k = 0. \tag{B.4}$$

According to the condition (2.26), we have $J_1 + J_2 + J_k = \text{even}$, leading to $(-1)^{J_1+J_2+J_k} = 1$. Hence, Eq. (2.3) is recovered.

B.2 Derivation of Eq. (2.10) and (2.11)

Applying Eqs. (A.10) and (A.9), we obtain

$$\begin{aligned}
& \sum_{M_1 M_2} \begin{pmatrix} J_1 & J_2 & J_k \\ M_1 & M_2 & M_k \end{pmatrix} Y_{J_1 M_1}(\hat{\mathbf{r}}) Y_{J_2 M_2}(\hat{\mathbf{r}}) \\
&= \sum_{M_1 M_2} \begin{pmatrix} J_1 & J_2 & J_k \\ M_1 & M_2 & M_k \end{pmatrix} \sum_{\ell' m'} \sqrt{\frac{(2J_1+1)(2J_2+1)(2\ell'+1)}{4\pi}} \begin{pmatrix} J_1 & J_2 & \ell' \\ M_1 & M_2 & m' \end{pmatrix} Y_{\ell' m'}^*(\hat{\mathbf{r}}) \begin{pmatrix} J_1 & J_2 & \ell' \\ 0 & 0 & 0 \end{pmatrix} \\
&= \sum_{\ell' m'} \sqrt{\frac{(2J_1+1)(2J_2+1)}{4\pi(2\ell'+1)}} Y_{\ell' m'}^*(\hat{\mathbf{r}}) \begin{pmatrix} J_1 & J_2 & \ell' \\ 0 & 0 & 0 \end{pmatrix} \sum_{M_1 M_2} (2\ell'+1) \begin{pmatrix} J_1 & J_2 & J_k \\ M_1 & M_2 & M_k \end{pmatrix} \begin{pmatrix} J_1 & J_2 & \ell' \\ M_1 & M_2 & m' \end{pmatrix} \\
&= \sum_{\ell' m'} \sqrt{\frac{(2J_1+1)(2J_2+1)}{4\pi(2\ell'+1)}} Y_{\ell' m'}^*(\hat{\mathbf{r}}) \begin{pmatrix} J_1 & J_2 & \ell' \\ 0 & 0 & 0 \end{pmatrix} \delta_{\ell' J_k} \delta_{m' M_k} \\
&= \sqrt{\frac{(2J_1+1)(2J_2+1)}{4\pi(2J_k+1)}} Y_{J_k M_k}^*(\hat{\mathbf{r}}) \begin{pmatrix} J_1 & J_2 & J_k \\ 0 & 0 & 0 \end{pmatrix}, \tag{B.5}
\end{aligned}$$

where we can define the coefficient as

$$a_{J_1 J_2 J_k} \equiv \sqrt{\frac{(2J_1+1)(2J_2+1)}{4\pi(2J_k+1)}} \begin{pmatrix} J_1 & J_2 & J_k \\ 0 & 0 & 0 \end{pmatrix}. \tag{B.6}$$

Hence, Eqs. (2.10) and (2.11) are demonstrated.

C Proof of Feasibility of Series Expansion

In this section we will prove the series expansion of $\bar{A}(k, \mu_n)$ and $\bar{B}(k, \mu_n)$ are feasible. Suppose p_1, p_2 are non-negative integers, we want to show the following finite series expansion always exists,

$$D(k, \mu_n) \equiv \int \frac{d^3 \mathbf{q}_1}{(2\pi)^3} (\hat{\mathbf{q}}_1 \cdot \hat{\mathbf{n}})^{p_1} (\hat{\mathbf{q}}_2 \cdot \hat{\mathbf{n}})^{p_2} = \sum_{i=0} D_i(k) \mu_n^i. \tag{C.1}$$

In spherical coordinates where the z -axis is chosen along $\hat{\mathbf{k}}$ and $\hat{\mathbf{n}}$ on the $x-z$ plane, the kernel will be

$$\begin{aligned}
F(p_1, p_2) &\equiv (\hat{\mathbf{q}}_1 \cdot \hat{\mathbf{n}})^{p_1} (\hat{\mathbf{q}}_2 \cdot \hat{\mathbf{n}})^{p_2} \\
&= (\sin \theta_1 \sin \theta_n \cos \phi + \cos \theta_1 \cos \theta_n)^{p_1} (-\sin \theta_2 \sin \theta_n \cos \phi + \cos \theta_2 \cos \theta_n)^{p_2} \\
&= \sum_{r_1=0}^{p_1} \binom{p_1}{r_1} \sin^{r_1} \theta_1 \sin^{r_1} \theta_n \cos^{r_1} \phi \cos^{p_1-r_1} \theta_1 \cos^{p_1-r_1} \theta_n \\
&\quad \times \sum_{r_2=0}^{p_2} (-1)^{r_2} \binom{p_2}{r_2} \sin^{r_2} \theta_2 \sin^{r_2} \theta_n \cos^{r_2} \phi \cos^{p_2-r_2} \theta_2 \cos^{p_2-r_2} \theta_n \\
&= \sum_{r_1=0}^{p_1} \sum_{r_2=0}^{p_2} (-1)^{r_2} \binom{p_1}{r_1} \binom{p_2}{r_2} \cos^{r_1+r_2} \phi \sin^{r_1} \theta_1 \sin^{r_2} \theta_2 \sin^{r_1+r_2} \theta_n \cos^{p_1-r_1} \theta_1 \cos^{p_2-r_2} \theta_2 \\
&\quad \times \cos^{p_1+p_2-r_1-r_2} \theta_n. \tag{C.2}
\end{aligned}$$

Averaging over the azimuthal angle ϕ , we are only left with terms with $r_1 + r_2 = \text{even}$, since $\langle \cos^m \phi \rangle_\phi = 0$ for odd integer m . The kernel then becomes

$$\begin{aligned} \langle F(p_1, p_2) \rangle &= \sum_{r_1=0}^{p_1} \sum_{r_2=0}^{p_2} (-1)^{r_2} \binom{p_1}{r_1} \binom{p_2}{r_2} \langle \cos^{r_1+r_2} \phi \rangle \sin^{r_1} \theta_1 \sin^{r_2} \theta_2 \cos^{p_1-r_1} \theta_1 \cos^{p_2-r_2} \theta_2 \\ &\quad \times (1 - \mu_n^2)^{\frac{r_1+r_2}{2}} \mu_n^{p_1+p_2-r_1-r_2} . \end{aligned} \quad (\text{C.3})$$

Since $(r_1 + r_2)/2$ and $p_1 + p_2 - r_1 - r_2$ are both non-negative integers, we can further expand it as a polynomial of μ_n . Thus, the expansion (C.1) is always feasible.

Furthermore, from Eq. (C.3) we obtain two properties of the expansion:

1. The power of μ_n goes up to $p_1 + p_2$, so that the series is finite. And it goes as $p_1 + p_2 - 2, p_1 + p_2 - 4, \dots$, down to 0 or 1 depending on the parity of $p_1 + p_2$.
2. The part with $\cos^{p_1-r_1} \theta_1 \cos^{p_2-r_2} \theta_2$ can always be written as products of Legendre polynomials of μ_1 and μ_2 . The only apparent problem comes from $\sin \theta_1$ and $\sin \theta_2$. However, since $r_1 + r_2$ is even, $r_1 - r_2$ must be even as well. Suppose $r_1 \geq r_2$, the potentially problematic term becomes:

$$\begin{aligned} \sin^{r_1} \theta_1 \sin^{r_2} \theta_2 &= (\sin \theta_1 \sin \theta_2)^{r_2} \sin^{r_1-r_2} \theta_1 \\ &= (\cos \theta_1 \cos \theta_2 - \hat{\mathbf{q}}_1 \cdot \hat{\mathbf{q}}_2)^{r_2} (1 - \cos^2 \theta_1)^{\frac{r_1-r_2}{2}} , \end{aligned} \quad (\text{C.4})$$

so that each term can be written in terms of the products of $\cos \theta_1, \cos \theta_2$ and $\hat{\mathbf{q}}_1 \cdot \hat{\mathbf{q}}_2$, which can be further decomposed into Legendre polynomials.